Disclaimer

This is a problem set (as turned in) for the module physics601.

This problem set is not reviewed by a tutor. This is just what I have turned in.

All problem sets for this module can be found at
http://martin-ueding.de/de/university/msc_physics/physics601/.

[disclaimer]

Lab report

Analysis of Z_0 decays

Experiment E213 – Universität Bonn

Martin Ueding
mu@martin-ueding.de

Lino Lemmer
l2@uni-bonn.de

2016-03-02

Tutor: David Hohn

In this experiment we analyze data from electron positron collisions collected with the OPAL detector at the LEP collider. Aim of the experiment is to have an insight in methods of data analysis in high energy physics.

In the first part we learn to distinguish between the different decay channels of the Z^0 boson by their signature in the detector with a small data sample.

In the second part we want to find mass, decay width and partial cross section of the Z^0 for different decay channels and the weak mixing angle angle from the forward backward asymmetry of the $e^-e^+ \to \mu^-\mu^+$ reaction. We also want to verify the lepton universality and identify the number of neutrino generations. For this part we use preselected data and Monte Carlo events as help.

Contents

Permission to upload

I, Martin Ueding, would like to scan and upload this lab report with your corrections to my website martin-ueding.de. There, the original lab report as well as the reviewed one will be licensed under the "Creative Commons Attribution-ShareAlike 4.0 International License". Is that okay with you?

Yes ☐ No ☐

1. Theory

1.1. The standard model of particle physics

In the standard model there are generally two types of elementary particles, fermions with spin $s = 1/2$ and bosons with spin $s = 1$. Within the fermions, there are particles which exist freely (leptons) and ones which only exist in bound states with each other (quarks). The latter make up heavier particles (hadrons) like the two quarks particles called mesons and baryons consisting from three quarks.

The leptons are organized into three generations of particles. In every generation one can find one charged particle with $q = -e$. These are the electron e^-, the muon μ^- and the tauon τ^-. To each one of them there belongs a very light uncharged neutrino $\nu_{e/\mu/\tau}$.

Within the quarks one also can find three generations. The first generation contains the up quark u and the down quark d. In the second one there are charm c and strange s and in the third one one can find the top and the bottom quark. All quarks carry electrical charge and mass.

Grouping the elementary fermions into weak isospin doublets, we have the following particles:

$$\begin{pmatrix} u_L \\ d_L \end{pmatrix} \quad \begin{pmatrix} c_L \\ s_L \end{pmatrix} \quad \begin{pmatrix} t_L \\ b_L \end{pmatrix} \qquad u_R \quad d_R \quad s_R \quad c_R \quad b_R \quad t_R\,,$$
$$\begin{pmatrix} \nu_{e,L} \\ e^-_L \end{pmatrix} \quad \begin{pmatrix} \nu_{\mu,L} \\ \mu^-_L \end{pmatrix} \quad \begin{pmatrix} \nu_{\tau,L} \\ \tau^-_L \end{pmatrix} \qquad e^-_R \quad \mu^-_R \quad \tau^-_R\,.$$

There are no right-handed neutrinos, at least they do not couple to the nuclear forces we know today.

All these particles interact through different interaction types: gravity, electromagnetic interaction, weak interaction and strong interaction. The first one plays no role in particle physics. The strong interaction acts only on the quarks and is mediated by gluons, the first type of bosons. The electromagnetic interaction acts only on electrically charged particles and the weak interaction on all left-handed fermions.

The electroweak interaction is a combination of the latter two interaction types. Speaking of symmetries, we combine the SU(2) symmetry of the weak interaction with its three interaction particles W^0, W^1 and W^2 with the U(1) symmetry of the electromagnetic interaction with its particle B^0 to get two charged bosons $W^\pm$ and two uncharged ones, γ and Z^0. The latter are superpositions of W^0 and B^0. The angle between the γ and the Z^0 in the W^0-B^0 plane is called weak mixing angle. Sometimes this is also called “Weinberg angle”, but although Weinberg did many things, this angle was introduced by somebody else first.

The Z^0 obtains its mass from the spontaneous symmetry breaking of the complex Higgs doublet. Its mass is 91.182 GeV, we will obtain a similar value from our analysis later on. A particle can only decay into particles which are lighter than it. This is demanded by four-momentum conservation. Compared to the Z-boson, light particles are all the leptons. The top-quark is heavier, therefore it cannot be a decay product. Left are the five other quarks (up, down, strange, charm, bottom).

1.2. Interaction of particles with matter

1.2.1. Photons

At different photon energies, different interactions are dominant. At high energy, the pair production is the most likely process. For this the photon needs an energy equal to the rest mass of the particle-antiparticle pair or higher. Below this energy Compton scattering and the photo effect are dominant. In these processes the photons lose their energy to electrons or other particles and are very important for particle detection in scintillators.

1.2.2. Charged particles

From all the processes that charged particles can undergo — inelastic scattering with orbiting electrons, elastic scattering with the nucleus, energy loss due to Cerenkov radiation or bremsstrahlung — the last is the most important for our case. Bremsstrahlung occurs when a charged particle gets accelerated in an Coulomb potential. The energy loss is highly dependent on the particle's mass:

$$\frac{\mathrm{d}E}{\mathrm{d}x} \propto \frac{1}{m^2}.$$

This is the reason why this effect is most relevant for the light electrons rather than the heavier muons.

1.3. Decay channels of the Z^0 boson

Since the Z^0 does not carry any type of electric charge, it only decays into fermion-antifermion pairs. Behavior and properties of possible decay products differ. The most obvious differences are between leptonic decay and hadronic decay.

1.3.1. Leptonic decay

The leptonic decay products, e^+e^-, $\mu^+\mu^-$ and $\tau^+\tau^-$ behave similar in the beginning. They fly apart collinear in opposite directions. Because of their high mass, the tauons decay very quickly through different decay channels listed in Table 1.1. The missing total energy is characteristic due to the great number of neutrinos created in these decays. Up to six charged tracks can be observed.

Decay channel	Probability/%	n-charged
$\pi^-\pi^0\nu_\tau$	24.0(6)	1
$e^-\bar{\nu}_e\nu_\tau$	17.9(3)	1
$\mu^-\bar{\nu}_\mu\nu_\tau$	17.6(3)	1
$\pi^-\nu_\tau$	11.6(4)	1
$\pi^-\pi^-\pi^+\nu_\tau$	5.6(7)	3
$\pi^-\pi^-\pi^+\pi^0\nu_\tau$	4.4(16)	3
$\pi^-\pi^0\pi^0\pi^0\nu_\tau$	3.0(27)	1

Table 1.1.: Most likely decay channels of a τ^- according to the manual.

The muons are lighter than the tauons, so they will not decay fast. Hence there will be only two charged tracks. Since they are still heavier than electrons, they interact only very little with matter. They only lose a small amount of energy in the detector.

Electrons are the lightest charged leptons. They loose a lot of energy in matter due to bremsstrahlung. As this bremsstrahlung can produce another electron positron pair, the number of charged tracks does not have to be exactly two.

The pair production (s-channel) is not the only way to get an electron positron pair. Elastic e^+e^- scattering, so called Bhabha scattering or t-channel scattering, is for small scattering angles the dominant process and has to be calculated out to get only decay products of Z^0.

The last leptonic decay is the neutrino pair production. Since they only interact weakly with matter, they most likely will not be detected.

1.3.2. Hadronic decay

The most obvious difference of hadronic decay compared to leptonic decay is the fact that quarks also interact through the strong interaction.

After the quark–antiquark pair is produced, the particles fly (like the leptons) in opposite directions. Due to the confinement, only color singlets can move freely. Particles with a net color charge are therefore strongly bound. The binding energy will increase with distance until a new real quark–antiquark pair is created from the vacuum. This happens more than once so that it will produce a whole bunch of quarks and antiquarks which result mostly in mesons. So there will be a lot of charged tracks in the detector.

1.4. The OPAL detector

The OPAL detector is one of four detectors of the “Large Electron Positron storage ring” LEP at the CERN in Geneva, Switzerland.

OPAL consists of an central detector with a vertex chamber, jet- and Z-chambers. These are built differently but have all the same function: tracking charged particles. From the signal in the vertex chamber one can extrapolate the point of collision. With this one find out if detected particles are produced in the detector or coming from cosmic rays. While the jet chamber has

a good radial resolution, the Z-chamber resolves the z coordinate accurately. Both provide information about the total momenta of charged particles by the curvature of the particle's tracks in an external magnetic field.

The central detector is surrounded by two calorimeters. Since "electromagnetic calorimeter" and "hadronic calorimeter" is quite a mouthful, we will call them e-cal and h-cal from now on. The e-cal consists of lead glass blocks with attached detecting plates. Here electrons and positrons loose energy due to bremsstrahlung. Emerging photons produce additional electron-positron pairs, which again loose their energy. Through this particle shower all the energy is deposited in the calorimeter. Hadrons lose only a part of their energy in the e-cal. The rest is released through another particle shower in the h-cal, which consists of alternating layers of iron and detector chambers. Since muons only loose a small part of their energy in the calorimeters, the whole setup is surrounded by another drift chamber. Here again charged particles, usually muons, are tracked. Therefore it is called muon chamber. However also cosmic particles can be detected here.

Another calorimeter, the f-cal ("forward calorimeter") is used to measure the luminosity. These are attached close to the beam pipes at both ends of the detector and consist of a few lead glass and wire chamber layers.

2. Exercises

There are a couple of exercises that are supposed to be done before the experiment.

2.1. Decay width

We are to compute the decay width Γ of a Z^0 particle into a pair of various fermions. The top-quark is heavier than the gauge boson, therefore it cannot decay into a pair of top-quarks. The Feynman diagram corresponding to the decay is shown in Figure 2.1.

Equation (2.12) from the manual gives the decay with into flavor f to be

$$\Gamma_f = \frac{N_c^f \sqrt{2}}{12\pi} G_F M_{Z^0}^3 \left((g_v^f)^2 + (g_a^f)^2 \right) .$$

An attempt to derive this equation is given in Chapter B.

We can insert the various quantum numbers of particles, insert the constants and obtain the decay widths. The quantum numbers and our results are listed in Table 2.1. The Fermi coupling constant has the value $1.66 \times 10^{-11}\,\mathrm{GeV}^{-2}$, see Equation (2.1) in the manual.

2.2. Partial widths

In the previous section, we have computed the decay widths for each kind of particle. Now we have to group the various particles into families and add their partial widths.

Hadronic width The hadrons in the final state are the up, down, strange, charm and bottom quarks. Therefore we have two up-type and three down-type quarks which results in a width of $\Gamma_{\mathrm{had.}} = 1689\,\mathrm{MeV}$. The branching ratio here is 0.691.

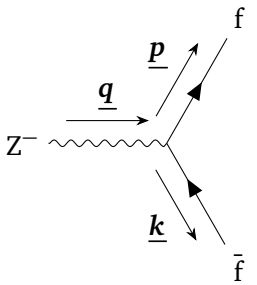

Figure 2.1.: Decay of a Z^0 gauge boson into a pair of fermions. Time is to the right.

Flavor	I_3	Q	N_c	Γ/MeV
Electron	$-1/2$	-1	1	84.1
Neutrino	$1/2$	0	1	167
Up-Quark	$1/2$	$2/3$	3	288
Down-Quark	$-1/2$	$-1/3$	3	371

Table 2.1.: Decay widths for the various families of fermions. As the fermions are taken to be massless, only one representative of the family is mentioned in the column "Flavor".

Type	Width / MeV	Branching ratio	Partial cross section / $10^{-11}\,\mathrm{MeV}^{-2}$
Hadronic	1689	0.691	10.8
Charged leptonic	252	0.103	1.61
Neutral leptonic	502	0.205	3.21
Total	2443	1	15.6

Table 2.2.: Partial decay widths, branching ratios and cross sections.

Charged leptonic width The charged leptons are the electron, the muon and the tauon. The charged leptonic width therefore is $\Gamma_{\text{ch.lep.}} = 252\,\text{MeV}$. The branching ratio here is 0.103.

Neutral leptonic width The neutral leptons are the electron-neutrino, the muon-neutrino and the tauon-neutrino. The neutral leptonic width therefore is $\Gamma_{\text{n.lep.}} = 502\,\text{MeV}$. The branching ratio here is 0.205.

Total width Summing all those widths up, we obtain $\Gamma_{\text{tot.}} = 2443\,\text{MeV}$.

All numerical values as well as the partial cross sections are in Table 2.2. The total cross section is

$$\sigma_{\text{total}}^{\text{peak}} = \frac{12\pi}{M_{Z^0}^2}\frac{\Gamma_e}{\Gamma_{Z^0}}\,.$$

2.3. Additional generation

If we have an additional generation, we have one more up-type and down-type quark. Also one more lepton-type and another neutrino-type. Therefore we need to add to the total width. The ratio is

$$\frac{\Gamma_{\text{total}} + \Gamma_e + \Gamma_\nu + \Gamma_u + \Gamma_d}{\Gamma_{\text{total}}} = 1 + \frac{\Gamma_e + \Gamma_\nu + \Gamma_u + \Gamma_d}{\Gamma_{\text{total}}} = 1.58\,.$$

We see that another generation of quarks and leptons significantly changes the total width and therefore also the total cross section.

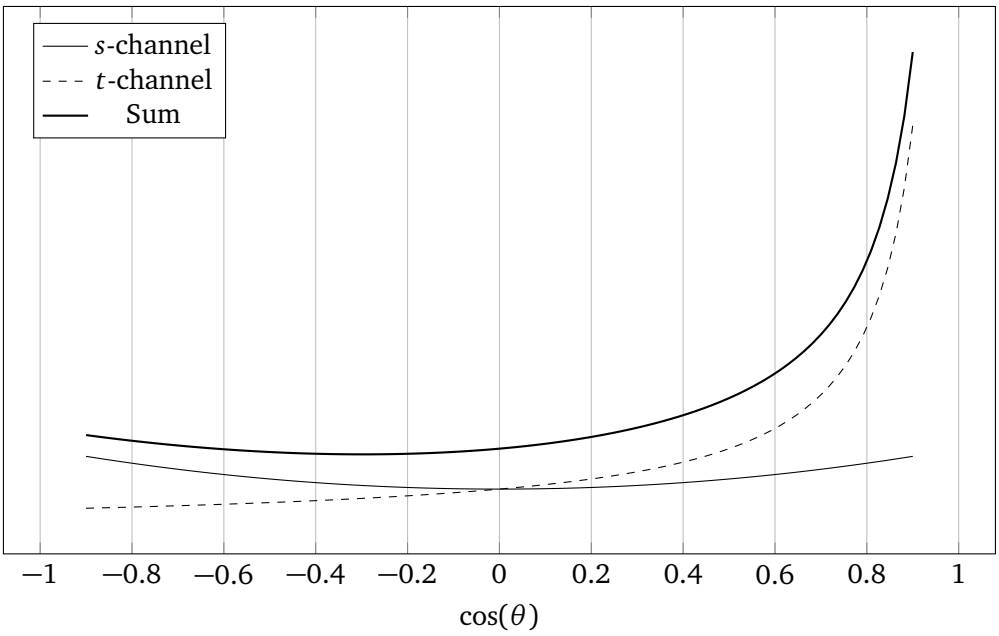

Figure 2.2.: Angular dependence of differential cross section in the s- and t-channel.

2.4. Angular dependence

As we can see from the tree-level QFT calculation for the Z^0 decay in the first problem, the angular dependence is indeed $(1+\cos(\theta)^2)$ as stated in the last paragraph on page 27 in the manual. This is the s-channel. For the t-channel the angular dependence is $(1-\cos(\theta))^{-1}$.

The reaction $e^+e^- \to \mu^+\mu^-$ only works in the s-channel. The reaction $e^+e^- \to e^+e^-$ works in both s- and t-channel.

All we have to do is to plot those two simple functions. The plots are shown in Figure 2.2. As written in the manual, the t-channel becomes dominant for very small angles, i.e. large $\cos(\theta)$.

2.5. Asymmetry

We are to compute the forward–backward asymmetry of the reaction $e^+e^- \to \mu^+\mu^-$. The given values for Mandelstam-s are 91.2 GeV, 89.2 GeV and 93.2 GeV. The values for the weak mixing angle in terms of $\sin(\theta_w)^2$ given are 0.210, 0.230 and 0.250. In total there are nine combinations, all are shown in Table 2.3.

The equation that we use is (2.19) from the manual:

$$A_{\mathrm{FB}}^f(s) \simeq -\frac{3}{2}\frac{a_e a_f Q_f \,\mathrm{Re}(\chi(s))}{(v_e^2+a_e^2)(v_f^2+a_f^2)},$$

where $\chi(s)$ is the propagator of the Z^0 boson as given in (2.11). It differs from the usual propagator of a vector particle and does not have any Lorentz structure. This is odd, we will

	A_{FB}^{μ}		
s	$\sin(\theta_{\mathrm{w}})^2 = 0.210$	$\sin(\theta_{\mathrm{w}})^2 = 0.230$	$\sin(\theta_{\mathrm{w}})^2 = 0.250$
91.2	−0.021 534	−0.023 426	−0.024 961
89.2	−0.021 057	−0.022 907	−0.024 407
93.2	−0.022 011	−0.023 946	−0.025 514

Table 2.3.: Forward–backward asymmetry A_{FB}^{μ} for different values of Mandelstam-s (rows) and different values of θ_{w} (columns).

just use the given propagator. The real part of that propagator has to be found by making the denominator real:

$$\chi(s) = \frac{s}{s - M_{\mathrm{Z}^0}^2 + \frac{\mathrm{i}s\Gamma_{\mathrm{Z}^0}}{M_{\mathrm{Z}^0}}} = s\frac{s - M_{\mathrm{Z}^0}^2 - \frac{\mathrm{i}s\Gamma_{\mathrm{Z}^0}}{M_{\mathrm{Z}^0}}}{\left(s - M_{\mathrm{Z}^0}^2\right)^2 + \left(\frac{s\Gamma_{\mathrm{Z}^0}}{M_{\mathrm{Z}^0}}\right)^2}.$$

The real part then is

$$\mathrm{Re}(\chi(s)) = \frac{s(s - M_{\mathrm{Z}^0}^2)}{\left(s - M_{\mathrm{Z}^0}^2\right)^2 + \left(\frac{s\Gamma_{\mathrm{Z}^0}}{M_{\mathrm{Z}^0}}\right)^2}.$$

Now we just need to insert all the numbers with $I_3 = -1/2$ and $Q = -1$ in both $f = \mathrm{e}$ and $f = \mu$.

3. Analysis

The data used in this lab experiment was gathered in the year 1992 and before. Therefore we only do analysis of the data. Part of the analysis is done at the university, the remainder is done at home. We will group our work by topic and not split by university and home.

3.1. Screening some decays

At first we look at some decays in the event display software GROPE. In order to learn the signatures of the various decays, we start with Monte Carlo datasets which only contain decays into a given channel.

The characteristics have different names within GROPE and PAW. Both are programming language identifiers and hard to read. Since we do not want to clutter our report with those identifiers, we use ones close to PAW but formatted nicer. See Table 3.1 for an overview.

Figure 3.1 shows a characteristic decay of each category (electrons, muons, tauons, hadrons) as displayed by GROPE. The electron decay in Figure 3.1a shows the typical back-to-back signature of two very fast (no curvature in the vertex chamber) charged particles. All the energy is deposited in the e-cal. In the dark blue header one can see that the missing energy is very small. The E-e-cal is pretty much identical with p-charged. Both energies are almost the beam energy.

Decays into muons have a different signature. The most prominent feature are the hits in the muon chambers, as one can see in Figure 3.1b. The p-charged is the beam energy, little energy is unaccounted for. This means that there are no neutrinos created in that decay. E-e-cal and E-h-cal is small, this is due to the big mass of the muon (compared to electrons).

Figure 3.1c shows a decay into tauons. This decay is not as simple as the previous ones. We have some missing energy (around a third), more than one charged track and also energy deposited into the various calorimeters. The missing energy comes from the neutrinos in the weak decay of the tauon. The number of charged tracks is still small (just five), therefore we can differentiate from the hadronic decays.

GROPE	PAW	Our name	Description
`Ctrk(N)`	`ncharged`	n-charged	Number of charged tracks
`Ctrk(Sump)`	`pcharged`	p-charged	Energy in charged tracks
`Ecal(SumE)`	`e_ecal`	E-e-cal	Energy in electric calorimeter
`Hcal(SumE)`	`e_hcal`	E-h-cal	Energy in hadronic calorimeter

Table 3.1.: Nomenclature used by GROPE, PAW and within this lab report.

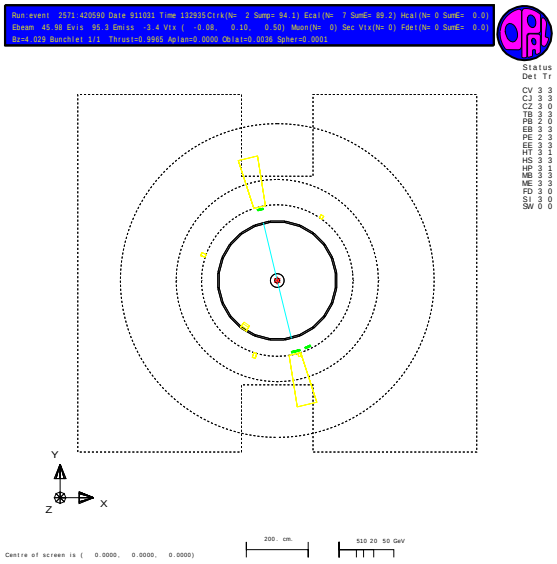

(a) Electrons

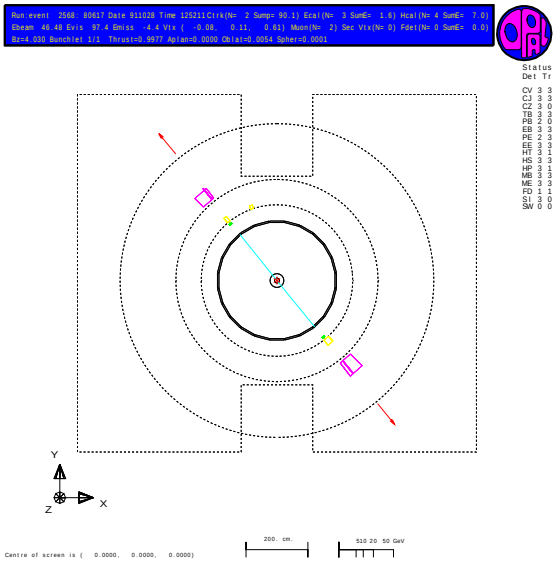

(b) Muons

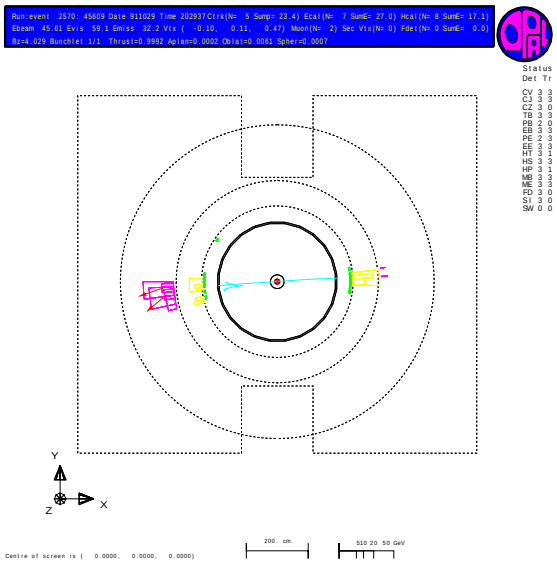

(c) Tauons

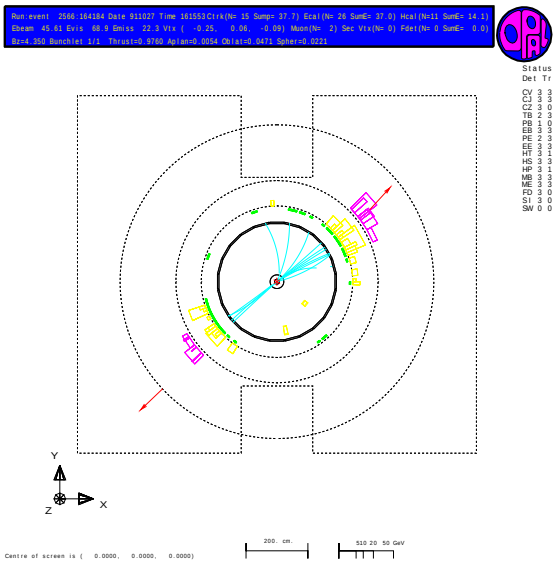

(d) Hadrons

Figure 3.1.: Event display of Monte Carlo events. One can see the traces from the vertex chamber in cyan, the hits in the e-cal are shown in yellow (probably hard to see on paper). In magenta, one has the hits in the h-cal. Muon penetrations are indicated with red arrows. Images are rendered with GROPE.

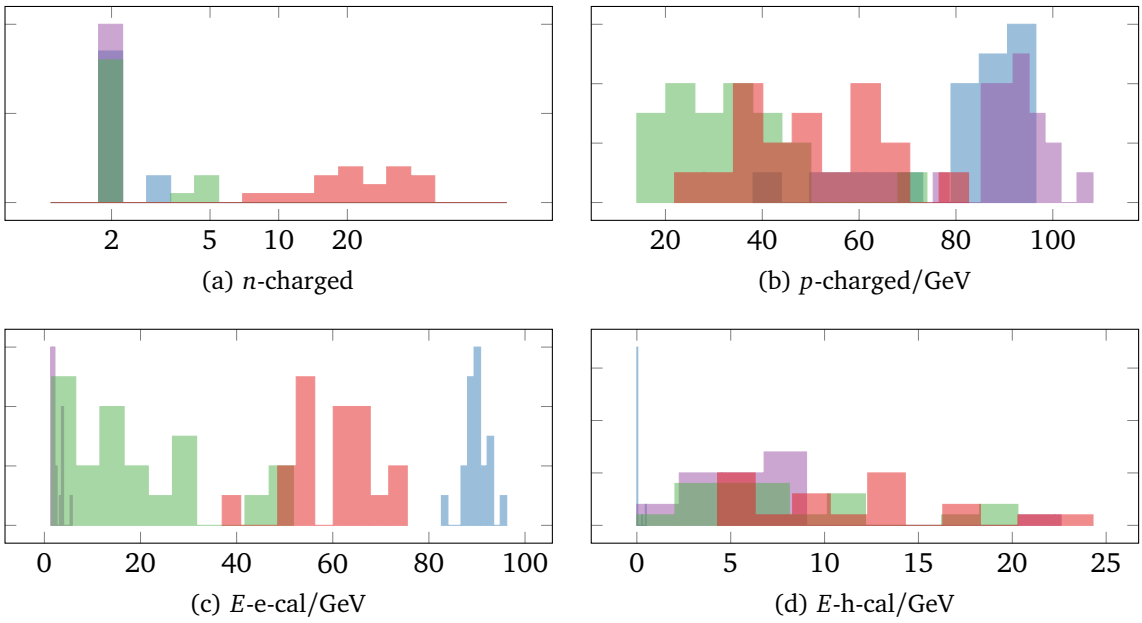

(a) n-charged (b) p-charged/GeV

(c) E-e-cal/GeV (d) E-h-cal/GeV

Figure 3.2.: Histograms with data gathered from Monte Carlo datasets in GROPE. The number of charged tracks is shown as a histogram with logarithmic bins.

Lastly, a decay into hadrons is shown in Figure 3.1d. One directly sees the large number of tracks, here 26, which exhibit a larger curvature. Also we have nonzero E-h-cal. Hadronic decays are easy to classify as their number of charged tracks is always rather large.

3.2. Defining the cuts

While reviewing the Monte Carlo events in GROPE, we generate histograms with the various characteristics. We choose to write down n-charged, p-charged, E-e-cal and E-h-cal. Those characteristics are also available in the later analysis of larger datasets using PAW.

3.2.1. Preliminary analysis

We will use the following color scheme throughout this report: Electrons, Muons, Tauons and Hadrons.

Using some twenty points per event class, we obtain the histograms shown in Figure 3.2. There one can see that some characteristics are well suited to cut the data. For instance in n-charged, we see that hadronic decays have more than seven tracks, whereas the leptonic decays have less. In the histogram for p-charged, we see that a cut at around 80 GeV can separate tauons and muons. Another cut in E-e-cal at around 75 GeV allows us to separate tauons and electrons. The energy deposited into the h-cal E-e-cal, is not very helpful for cutting.

Having those cuts in place, we take a look at the `test` datasets which are not sorted by event type. There we try to use our fresh intuition about the decay channels to identify the type of decay. Then we take a look at the characteristics and see whether our cuts would come to the

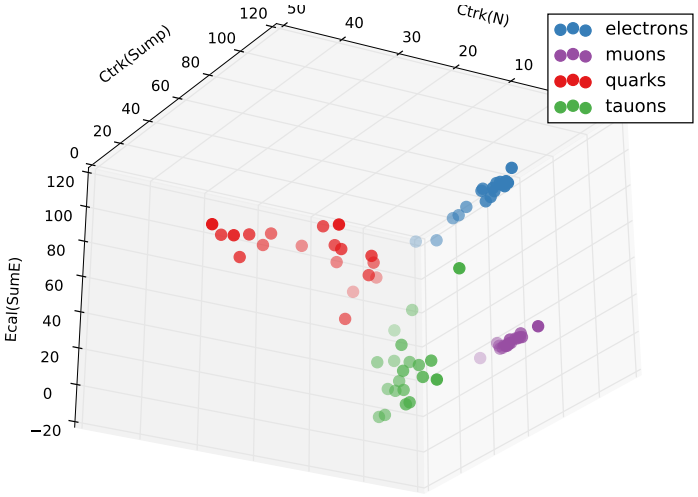

Figure 3.3.: 3D visualization of the three most expressive characteristics.

	Cut criterion			
Particle	n-charged	p-charged/GeV	E-e-cal/GeV	E-h-cal/GeV
Electrons	< 4		> 60	
Muons	< 4	> 75	< 20	
Tauons	< 7	< 75	≤ 75	
Hadrons	> 7			

Table 3.2.: Cuts derived from the few data points manually extracted from the Monte Carlo events.

same conclusion. For most decays, this worked out well. Some were not classified correctly; this is somewhat expected as we will never be able to avoid false-positives and false-negatives.

While we were trying to find suitable cuts, a 3D visualization like shown in Figure 3.3 was really helpful. There we could rotate the cloud of events in the characteristics space and see different clusters. Such a 3D-representation can hardly be printed and must be viewed interactively, though.

We would really have liked to perform this visualization with more data. Then one could even do a 3D-histogram and find cut surfaces which separate the data most cleanly. In PAW we are limited to hyperplanes anyway, so we just choose a few axis-parallel planes as they will do the job sufficiently well.

After the refining using events from the `test` dataset, we have the cuts listed in Table 3.2.

3.2.2. More data points

Our histograms are only filled with a limited amount of data. It would be wise to use more data to refine the cuts further. To that end, we change from the single event viewer GROPE to the analysis tool PAW which is a predecessor to ROOT.

We load the big Monte Carlo datasets into PAW and let it generate histograms with the characteristics. Sadly we only have the exported postscript documents and not the raw data. Therefore we can only present ill-looking plots in Figure 3.4. Although the labels are ridiculously small, we have crammed four plots on a single page; we would have needed four pages otherwise. If we had the raw data, we would have combined the four decay modes into a single histogram, just like what was done in Figure 3.2 with the manually collected data.

With a magnifying glass we can see that there are mostly two charged tracks for electron and muon decays. Interestingly, there are occasionally three to four tracks for the electron.

As expected from decay modes with hadrons, we see that tauons can have six charged tracks. Hadrons can also decay with six or less charged tracks, but the most part decays with more than ten tracks.

The other characteristics are also plotted using PAW. p-charged is shown in Figure A.1, E-e-cal in Figure A.2 and E-h-cal in Figure A.3.

3.2.3. Angular distribution

As one can see in Figure 3.5, the angular distribution of the four decay modes is not the shifted parabola as expected from the s-channel theory. For the electrons, this arises from the mixing with the t-channel. We do not want to include the t-channel reactions as this would make a comparison to the other leptonic channels (only s-channel there) impossible.

We have shown in Figure 2.2 how the s- and t-channel scale with the angle. At small angle, the unwanted t-channel dominates. Therefore we need to cut large $\cos(\theta)$ out of our analysis. The efficiency will go down, but the quality of the remaining data will be better. We also cut the peak at $\cos(\theta) < -0.9$ as we do not know its origin but know that it cannot come from a simple s-channel process.

The muons (see Figure 3.5b) look pretty good. At $|\cos(\theta)| > 0.9$ we have a sharp drop which we blame on the detector not covering the whole solid angle. Since the beam pipe needs to go through the detector, one cannot detect collinear events. We therefore cut those events away.

The shape of the tauons (see Figure 3.5c) seems to be a parabola in the middle but flatten off to the sides. Events with only one charged positive track have to be a decay into an positron or an anti-muon. A neutrino is created in those processes, skewing the angular distribution. Therefore this flattening does not need to be cut out as we have a physical explanation for it.

For the hadrons (see Figure 3.5d), an angular distribution is rarely defined, there is only one event that even has a well-defined θ-angle. Therefore we do not perform any cutting in the hadronic sector.

Our refined and final cuts including the angle are listed in Table 3.3.

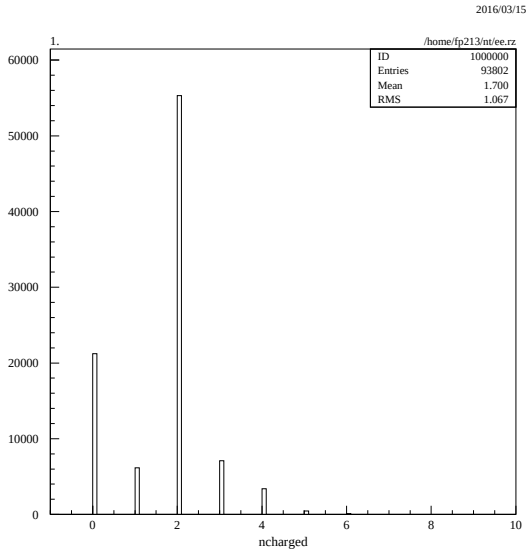

(a) Electrons

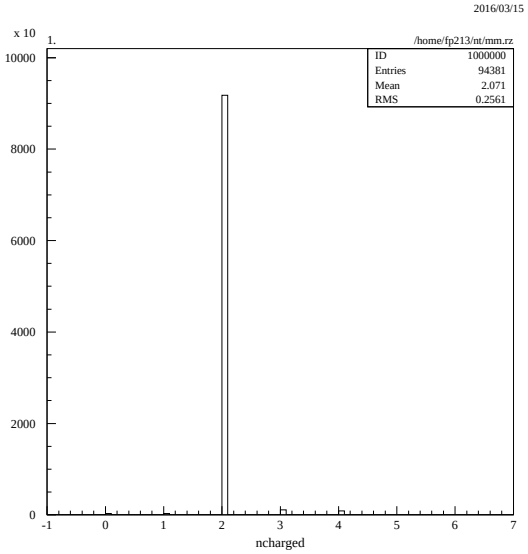

(b) Muons

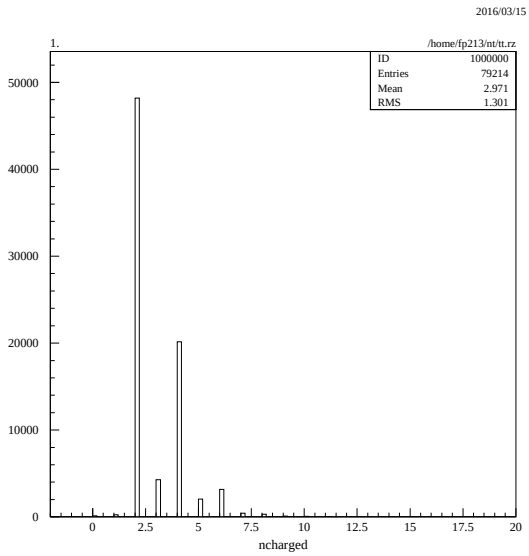

(c) Tauons

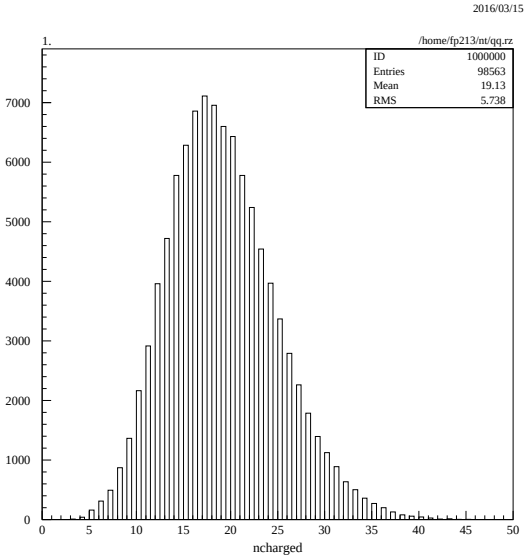

(d) Hadrons

Figure 3.4.: Number of charged tracks, n-charged, for the four decay types. Histograms generated with PAW from Monte Carlo datasets.

	Cut criterion				
Particle	n-charged	p-charged/GeV	E-e-cal/GeV	E-h-cal/GeV	$\cos(\theta)$
Electrons	< 4		> 60		$-0.9 \leq \cdots \leq 0.5$
Muons	< 4	> 75	< 20		$-0.9 \leq \cdots \leq 0.9$
Tauons	< 7	< 75	≤ 75		
Hadrons	> 7				

Table 3.3.: Cuts derived from the full Monte Carlo datasets.

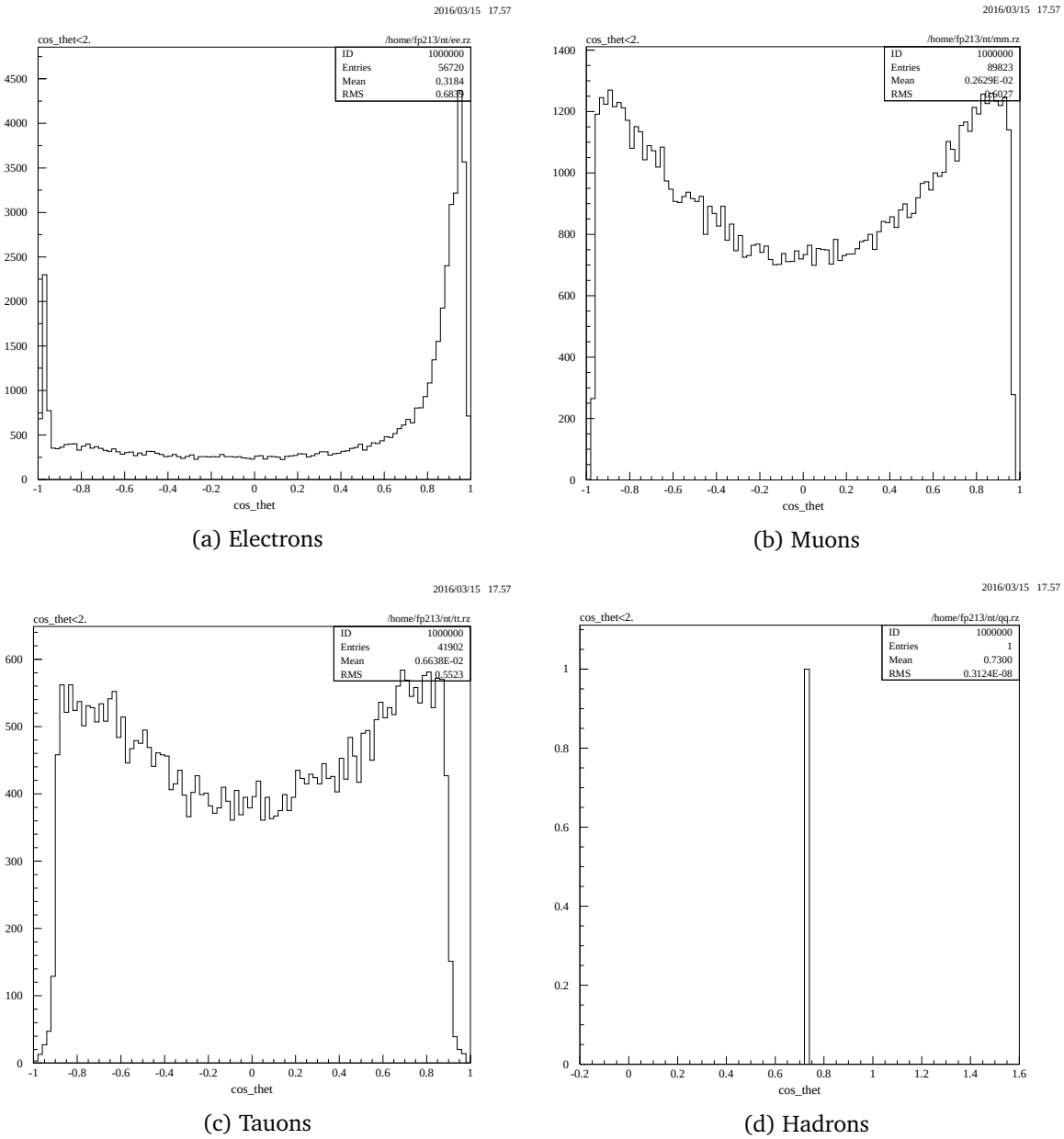

(a) Electrons

(b) Muons

(c) Tauons

(d) Hadrons

Figure 3.5.: Angular distribution with respect to cos(θ) for the four decay types. Histograms generated with PAW from Monte Carlo datasets. Events without a defined angle are excluded, therefore there are no events with more or less than one positively charged track included.

3.3. Bootstrap error estimation

The default method for error estimation is the *Gaussian error propagation*. This works by applying $[\Delta f\,](x) = |f'(x)| \cdot \Delta x$ for every transformation used. The implicit assumptions used here are that errors are both small and Gaussian throughout the analysis. Especially if one has a lot of analysis steps, the propagated error might be too large or small.

Besides being tedious, this scheme also does not provide any help when doing fits. Methods like the `scipy.optimize.curve_fit`, which we use here, will give a covariance matrix. Taking the square root of the diagonal usually gives a sufficient error estimate if the errors are uncorrelated, which is often the case. Although the function can perform an error-weighted fit, it does not incorporate the uncertainty of the input data into the error of the fit parameters (at least in older versions). Still, uncertainties in the categorical variable (usually x) are not included in this function.

A method to alleviate all those problems is the *bootstrap* method. It is an intrinsically numerical and statistical procedure. It is a "meta analysis of the data itself" in a sense. Instead of running our analysis once with the original data, we also run it a couple hundred times with slightly different datasets. This can be the same experiment conducted a couple more times. All the input values will be slightly different according to their statistical uncertainty. Running the analysis on all the different inputs, one obtains a distribution of final results. Taking the standard deviation of this distribution will be a robust estimation of the statistical error on the final results.

As one does not have to compute partial derivatives with respect to all input parameters, this method is very general and can be used for every step in the analysis, even curve fitting.

Here we do not have the luxury of multiple datasets. As the detection of particles essentially is a counting experiment, we assume that a value N is associated with a standard deviation of $\sqrt{N}$. We only have one data point, so we cannot do a bootstrap right away. Therefore we draw more data points from a Gaussian distribution centered on N with width $\sqrt{N}$. The values that we get should roughly be the same we would have gotten when performing the analysis with another data set.

This method sounds outrageous, we just pull more data "out of the hat" by doing this resampling. Gaussian error propagation does the same thing, really, just analytically. Therefore we are performing the same procedure, just with numerical methods and less assumptions.

Another aspect that one should cover in curve fitting is the dependence of the result on the number of data points used. In an ideal case we can remove any of the points and the fit would still give the same result. Later we will have fits with seven data points and see that removing any of the points will drastically alter the curve. In order to obtain this effect, we do a *Jackknife* in first order for the fits as well. Instead of fitting with all seven points, we randomly remove one of the points in each run of the fit. As we perform hundreds of bootstrap samples, the mean value will not be altered much. The standard deviation of the fit parameters will increase, just what we want for fragile fits. We will see this at the cross sections later on.

Usually, only one fit curve is given. The bootstrap method will also give us a distribution of fit curves which we plot as a band of curves. Correlation between the fit parameters will become directly visible.

Gaussian error propagation assumes that errors are symmetric around the mean value. In realistic examples, this might not be the case. We can obtain asymmetric errors using the percentiles of the bootstrapped distribution. This will be seen in the forward–backward asymmetry.

3.4. Muon forward–backward asymmetry

The muon forward–backward asymmetry is a quantity that we want to extract from the data. For this we need to filter the actual dataset (in our case number 1) for muons. Then we also need to filter by beam energy. The dataset contains seven different beam energies, we define seven more filters like the following:

```
nt/cuts $11 e_lep>44.0.and.e_lep<44.5
nt/cuts $12 e_lep>44.5.and.e_lep<45.0
```

Using those, we can filter the data for muons (`$2`), positive or negative angle (`cos_thet<0.` or `cos_thet>0`) and for the energy (`$11`). Printing this as a histogram, we use the following code:

```
nt/plot daten1.cos_thet $2.and.cos_thet<0..and.$11
pict/print afb-muons-daten1-negative-energy1.ps
nt/plot daten1.cos_thet $2.and.cos_thet>0..and.cos_thet<2..and.$11
pict/print afb-muons-daten1-positive-energy1.ps
```

We have also supplied the additional criterion for sensible angles (`cos_thet<2.`) because undefined angles have a numerical value way greater than two.

From the exported diagrams (not included in this report) we extract the number of events with $\cos(\theta) > 0$, which we call N_+, and the events with $\cos(\theta) < 0$, which we call N_-. The asymmetry is then simply

$$A_{\mathrm{FB}} = \frac{N_+ - N_-}{N_+ + N_-}\,.$$

Our analysis to this point is based on the tree level formalism. Higher order corrections are needed in every QFT for more accurate results. Here we are given the combined effect of all those corrections as a table of shift for A_{FB}. For each beam energy, we add the correction and obtain a final value for A_{FB}. The resulting asymmetries for the different beam energies are shown in Table 3.4 and Figure 3.6. Error estimation is done by assuming an error of $\sqrt{N}$ for all the counts and using resampling bootstrap for the final result.

3.4.1. Weak mixing angle

At the peak, the relation

$$A_{\mathrm{FB}}^{\mathrm{peak}} \simeq 3\left(\frac{v_l}{a_l}\right) \qquad \text{and} \qquad \frac{v_l}{a_l} = 1 - 4\sin(\theta_w)^2$$

$\sqrt{s}$	A_{FB}
88.5	−0.14(9)
89.5	0.04(7)
90.2	−0.14(6)
91.2	0.01(2)
92.0	0.03(4)
93.0	0.23(6)
93.7	0.19(6)

Table 3.4.: Forward–backward asymmetry in the muon events.

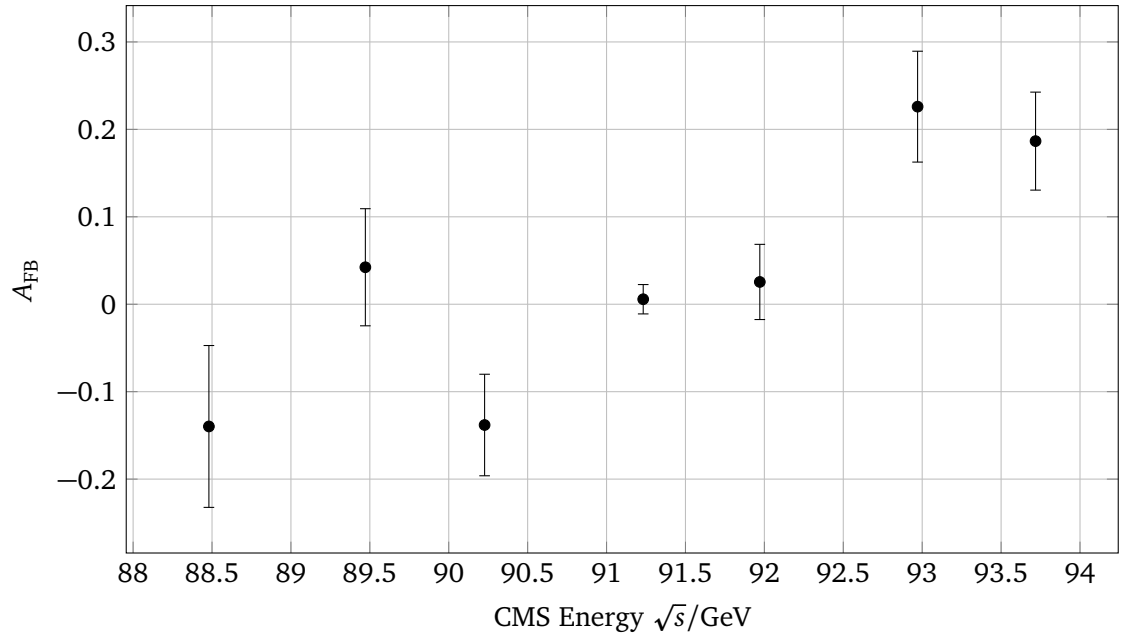

Figure 3.6.: Forward–backward asymmetry in the muon events. Shown are corrected values for A_{FB}.

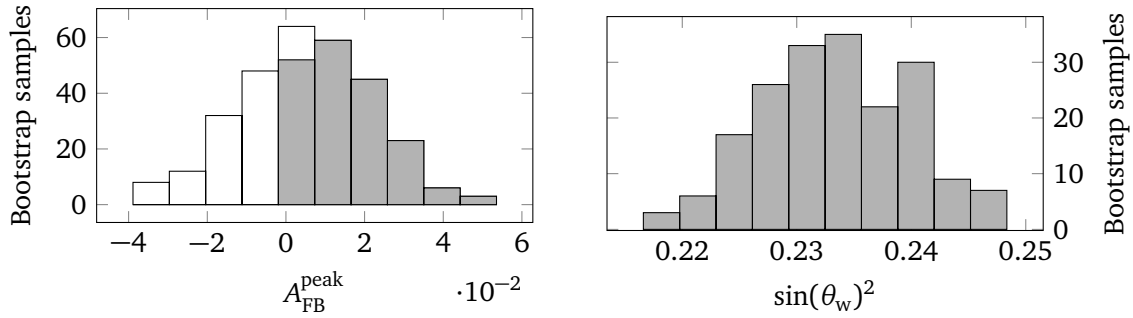

(a) Asymmetry values. Only the positive ones are actually taken, those are marked in gray.

(b) Weak mixing angle. The shape is quite symmetric but not centered around actual value.

Figure 3.7.: Histograms of the distributions used in the bootstrap error estimation.

holds for leptons. This expression is taken from the manual, Equation (2.21). Using the asymmetry value at the peak (fourth data point), we obtain $\sin(\theta_{\mathrm{w}})^2 = 0.239(7)$ from

$$\sin(\theta_{\mathrm{w}})^2 = \frac{1 - \sqrt{A_{\mathrm{FB}}^{\mathrm{peak}}/3}}{4}.$$

Due to the square root in the used relation, the bootstrap sampling can encounter illegal values which we just drop. The ratio of ignored values is 37.3 %, which is quite high. All values that are used are shown in Figure 3.7a. Although this seems bad, this only affected the error estimation. The distribution of resulting $\sin(\theta_{\mathrm{w}})^2$ values is shown in Figure 3.7b. One can see that is it rather symmetric but not centered around the value we obtain by computing with the actual input (not resampled). Therefore we conclude that we actually have a significant asymmetric error, namely $\sin(\theta_{\mathrm{w}})^2 = 0.239^{+0.001}_{-0.013}$.

3.5. Detection efficiency

By choosing the cuts in a particular way, we make a compromise between detection efficiency and underground. Choosing a tight cut will discard events that should have been counted. This will lead to a loss of a certain fraction of events. This is not directly a problem as we can just compensate by this loss factor. However, our statistical errors will grow as we have less statistics. A loose cut will water the sorting with underground events. Say we want to filter out electrons but our cuts are too loose. Then some tauon events might slip into the electrons category.

Both types of errors, the false-negatives (inefficiency) and the false-positives (underground), can be handled using a detection matrix $\boldsymbol{D}$ and Monte Carlo datasets. The Monte Carlo datasets are purely of one decay channel. Therefore we know exactly that we only have, say, electrons. Applying our cuts to the Monte Carlo electrons, we will see how many are actually detected as electrons. This is our efficiency. Then we take the other three kinds (muons, tauons, hadrons) of the Monte Carlo datasets and apply the electron cuts to it. Ideally, we should not get any events. The ratio of other events that we falsely identify as electrons is the underground.

Using a linear model for this, we need a mapping from the actual events vector $\boldsymbol{A}$ (in electron-muon-tauon-hadrons space, $\mathbf{N}^4$) to the identified events vector $\boldsymbol{I}$ (same space). The detection

	Acceptance rate / %			
Detected as	Electrons	Muons	Tauons	Hadrons
Electrons	21.7(1)	0.001(1)	1.28(4)	0.00
Muons	0.00	84.0(3)	0.10(1)	0.00
Tauons	2.77(6)	9.2(1)	96.8(4)	0.50(2)
Hadrons	0.006(3)	0.00	0.69(3)	99.0(3)

Table 3.5.: The detection matrix $\boldsymbol{D}$. Although it is displayed in a table, it is meant as a matrix which can be right-multiplied with an actual events vector $\boldsymbol{A}$. The resulting vector will be the vector of identified events $\boldsymbol{I}$ of our cuts. The matrix is mostly diagonal, the low number for electron–electron is due to our mistake in angular restriction (see text).

matrix is then defined via $\boldsymbol{I} = \boldsymbol{DA}$. In order to find the sixteen matrix elements, we apply four four-vectors with Monte Carlo events, one for each decay type.

3.5.1. Determining matrix elements

In order to do this with PAW, we define our final cuts for electrons, muons, tauons and hadrons:

```
nt/cuts $1 ncharged<4.and.e_ecal>60.and.cos_thet<.5.and.cos_thet>-0.9
nt/cuts $2 pcharged>75.and.ncharged<4.and.e_ecal<20.and.cos_thet<.9.and.cos_thet>-0.9
nt/cuts $3 pcharged<75.and.ncharged<7.and.e_ecal<75
nt/cuts $4 ncharged>7
```

We need to count the number of events that matched a given cut. Creating a histogram with respect to an arbitrary characteristic will give us this number as a side effect. The following generates a histogram with electron data and the electron filter:

```
nt/plot electrons.ncharged $1
pict/print matrix-electrons-with-electron-filter.ps
```

And this generates a histogram with muon data and the same filter:

```
nt/plot muons.ncharged $1
pict/print matrix-muons-with-electron-filter.ps
```

Similar expressions are needed for the other matrix element, in total we need 16 of those counting histograms. The resulting histograms are shown in Figure A.4. Squint at the row "Entries" in the legend, this is the interesting number.

For the electrons, the Monte Carlo input vector is $\boldsymbol{A} = (94381, 0, 0, 0)^{\mathrm{T}}$. Then we look at the output in the four histograms and find $\boldsymbol{I} = (20474, 1, 1013, 0)^{\mathrm{T}}$. From this, we can construct the first column in the matrix. Using the other filters, we can construct the whole matrix. Table 3.5 shows the matrix. It can be seen that it is mostly diagonal, just as we want it to be. The detection efficiency for the electrons is not very great. This comes from the severe cutting in $\cos(\theta) < 0.5$ which discards a lot of events.

	Correction factor			
Actually are	Electrons	Muons	Tauons	Hadrons
Electrons	4.62(3)	0.0066(1)	−0.061(1)	0.000 31(1)
Muons	0.000 16(2)	1.191(4)	−0.0013(1)	0.000 006 4(8)
Tauons	−0.132(2)	−0.1129(9)	1.035(4)	−0.0052(2)
Hadrons	0.000 62(8)	0.000 78(3)	−0.0072(3)	1.010(3)

Table 3.6.: The inverted detection matrix $\boldsymbol{D}^{-1}$.

The errors given in the matrix are the assumed $\sqrt{N}$ standard deviation from a counting experiment.

3.5.2. Inverting the matrix

We need to invert the matrix in order to use this detection matrix $\boldsymbol{E}$ as a correction. This will be numerically stable as it is almost diagonal. The inverted matrix is shown in Table 3.6. The errors for the matrix elements come directly from the bootstrapping.

3.5.3. Conceptual mistake

There is one mistake that we did in the derivation of the matrix, and we cannot recover from this after the fact. The matrix was set up using the final cuts, which also means that we only allow $\cos(\theta) \leq 0.5$ in the electrons. We did that to filter out the t-channel. As one can see in the inverse detection matrix in Table 3.6, the correction factor for the electron–electron case is around 4.6. This is way larger than the other diagonal elements. The matrix element is this large as we have made a severe cut and filtered out most of the electron events. In contrast to the other channels, this is something we actually want in order to get rid of the t-channel!

Using the matrix $\boldsymbol{D}^{-1}$ now, the t-channel will come back, at least from the numbers. Therefore we will find later on that the cross sections of the scattering into electrons. Table 3.11 and Figure 3.8 clearly show this apparent violation of lepton universality.

This is an overcompensation in our correction, we should have also cut the Monte Carlo data in the angle. The Monte Carlo data contains t-channel events as well, which we also do not want. By taking the ratio of filtered electrons and unfiltered Monte Carlo electrons, our acceptance ratio will correct the t-channel back in. We should actually have filtered the Monte Carlo with the same $\cos(\theta) \leq 0.5$ cut in order to have a reduced number of false-negatives and therefore no overcompensation. We do not have access to the machines running PAW now, so we can just explain why the results do not come out right and use the values for the muons as an replacement, *assuming* that lepton universality does hold.

	Raw count			
$\sqrt{s}$/GeV	Electrons	Muons	Tauons	Hadrons
88.5	138(12)	124(11)	482(22)	3526(61)
89.5	220(15)	218(15)	490(23)	5329(75)
90.2	247(17)	311(19)	437(23)	7548(96)
91.2	2588(49)	3502(58)	5485(72)	92 766(296)
92.0	394(20)	626(25)	912(30)	15 291(122)
93.0	155(13)	232(16)	473(22)	6642(83)
93.7	206(14)	302(17)	532(22)	7421(82)

Table 3.7.: Raw counts for the four decay types and seven beam energies.

3.6. Partial cross sections

3.6.1. Counts

In order to compute cross sections, we need count rates. We filter the dataset with our cuts and an energy selection. For instance in the following snippet we use the muon filter (`$2`) with the third beam energy (`$13`):

```
nt/plot daten1.ncharged $2.and.$13
pict/print filtered-daten1-as-muon-energy3.ps
```

We look at the generated histograms and extract the number of events from each histogram. The results are collected in Table 3.7. Shown are the errors which we assume to be $\sqrt{N}$ as this is a counting experiment. Those errors are also used for resampling.

The counts are just the ones left after applying the cuts. As argued in regarding the detection efficiency (c.f. Section 3.5), those counts include some number of false-positives (underground) and false-negatives (inefficiency). Therefore we need to correct for that with the inverse matrix derived above.

Taking the four counts at each beam energy as an "identified events" vector $\boldsymbol{I}$, we can use $\boldsymbol{D}^{-1}$ to give us the "actual events" vector $\boldsymbol{A}$. We do this for each of the seven beam energies and obtain the corrected counts. Those are shown in Table 3.8. Again, we have overcompensated the correction for the electrons.

3.6.2. Incorporating the luminosity

We want to compute the partial cross sections, those are the cross sections of the individual decay channels. For this we just need to take the number of counts in each channel and divide by the integrated luminosity. Therefore we have

$$\sigma_i = \frac{N_i}{\int \mathrm{d}t\, \mathscr{L}}\,.$$

	Corrected count			
$\sqrt{s}$/GeV	Electrons	Muons	Tauons	Hadrons
88.5	607(55)	147(14)	448(20)	3559(63)
89.5	990(70)	259(18)	426(20)	5381(79)
90.2	1118(80)	370(23)	346(20)	7624(98)
91.2	11 664(244)	4164(71)	4454(80)	93 698(411)
92.0	1774(90)	745(30)	741(27)	15 444(132)
93.0	689(58)	275(19)	408(19)	6708(86)
93.7	923(62)	359(20)	451(20)	7495(86)

Table 3.8.: Corrected counts for the four decay types and seven beam energies.

$\sqrt{s}$/GeV	$\int \mathrm{d}t\, \mathscr{L}/\mathrm{nb}^{-1}$
88.5	676(6)
89.5	544(5)
90.2	420(4)
91.2	3122(22)
92.0	640(6)
93.0	479(4)
93.7	767(6)

Table 3.9.: Integrated luminosities $\int \mathrm{d}t\, \mathscr{L}$ for the seven beam energies. The values are taken from the experiment description, the error is the total error (combined statistical and systematic error).

Table 3.9 lists the integrated luminosities for our dataset taken from the manual. As the luminosities also have an error associated with them, we will resample them as well in order to incorporate the error in our results.

3.6.3. Cross sections

Using the relation between the counts and luminosity, we can compute the partial cross section for each of the channels. The obtained cross sections need to be corrected by higher-order effects. Those are given to use as simple correction numbers, reproduced in Table 3.10. The results are shown in Table 3.11. Errors are the combined errors of luminosity, counts and matrix elements via the bootstrap method.

One can already see that for the central energies around M_{Z^0}, the electron cross section is too large compared to the muons and tauons. This is due to our mistake in determining the electron matrix elements.

A graphical representation of the cross sections is shown in Figure 3.8. As the individual channels have very different height, the four channels are shown separately in Figure 3.9. The figures already feature the fitted function which we will turn to next.

	$\Delta\sigma$/nb	
$\sqrt{s}$/GeV	Hadrons	Leptons
88.5	2.00	0.0900
89.5	4.30	0.200
90.2	7.70	0.360
91.2	10.8	0.520
92.0	4.70	0.220
93.0	−0.200	−0.0100
93.7	−1.60	−0.0800

Table 3.10.: Radiative corrections for the cross sections as given in Table 5.5 from the manual.

	σ_i/nb			
$\sqrt{s}$/GeV	Electrons	Muons	Tauons	Hadrons
88.5	0.99(8)	0.31(2)	0.75(3)	7.3(1)
89.5	2.0(1)	0.68(3)	0.98(4)	14.2(2)
90.2	3.0(2)	1.24(6)	1.18(5)	25.9(3)
91.2	4.26(8)	1.85(2)	1.95(3)	40.8(3)
92.0	3.0(1)	1.38(5)	1.38(4)	28.8(3)
93.0	1.4(1)	0.56(4)	0.84(4)	13.8(2)
93.7	1.12(8)	0.39(3)	0.51(3)	8.2(1)

Table 3.11.: Cross sections for the four decay types and seven beam energies.

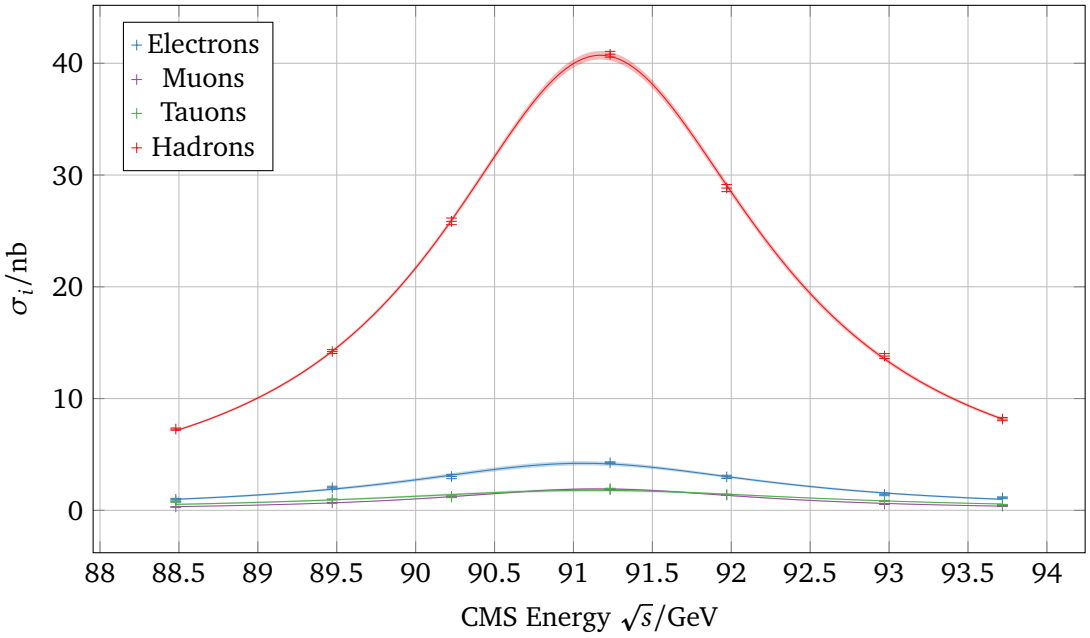

Figure 3.8.: Partial cross sections for each type of final state. One can see that the muon and tauon cross sections are similar, as expected. As we incorrectly correct for a t-channel, the electron cross section is too large.

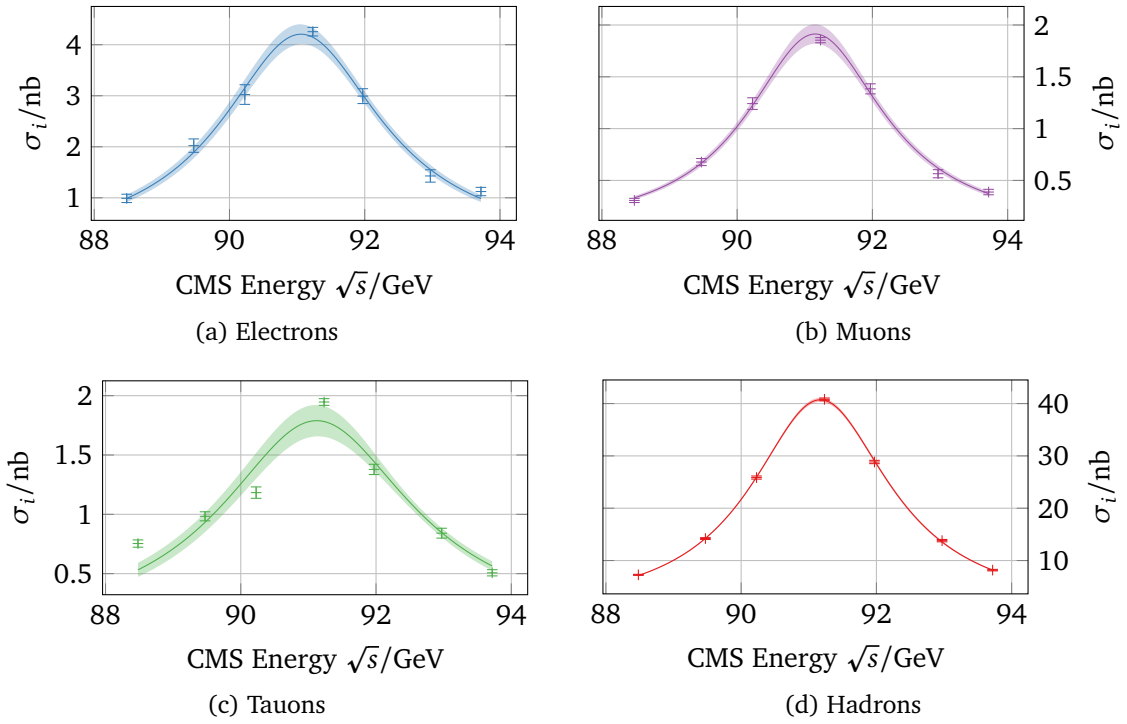

(a) Electrons (b) Muons

(c) Tauons (d) Hadrons

Figure 3.9.: Zoom-in of Figure 3.8. One can see the different qualities of the data points and the fits.

3.7. Decay widths

3.7.1. Curve fitting

From the energy dependence of the cross sections, we can compute the decay width and the rest mass of the Z^0 gauge boson generated by the spontaneous symmetry breaking of the Higgs field. As the tree-level cross section contains the modulus squared of the propagator, the expected energy dependence is similar to that of a Lorentz curve,

$$\sigma_f \propto \frac{1}{M_{Z^0}^2} \frac{s}{(s - M_{Z^0}^2)^2 + (s^2 \Gamma_Z^2 / M_{Z^0}^2)},$$

taken from Equation (3.12) in the manual. We fit a curve to the partial cross sections for each decay channel. Luckily it is not 1992 any more and we can just do this ourselves at home.

As we use a bootstrap scheme for error calculation, we perform the fit a couple hundred times with resampled input data. This gives us a set of hundreds of different fit parameters and also fit curves. For each interpolation value of $\sqrt{s}$ in the resulting curve we take mean and standard deviation. The result is shown as an error band for each fit curve.

Additionally, we have the problem that we are limited to seven beam energies. This introduces another source of error that we control with a jackknife approach in the fitting. Instead of fitting all seven data points, we randomly leave one of them out and fit only the remaining six. This makes the fit still able to converge but simulates the effect that adding or removing another

Type	M_{Z^0}/GeV	Γ_Z/GeV	σ_f^{Peak}/nb
Electrons	91.08(5)	2.9(2)	4.2(2)
Muons	91.17(4)	2.5(1)	1.91(9)
Tauons	91.15(8)	3.5(4)	1.8(1)
Hadrons	91.19(1)	2.52(3)	40.7(4)

Table 3.12.: Fit parameters of the curves used in Figure 3.8 for the partial cross sections.

data point has. If a result changes when a single data point is removed, this should add to the uncertainty of the result. Our fit parameters, the mass and width of the Z-boson as well as the peak cross section, are shown in Table 3.12.

As one can see in Figure 3.9c, the three points in the low $\sqrt{s}$ area contribute a lot to the uncertainty of the fit. The jackknife method is dearly needed, as the error in width would have been underestimated by an order of magnitude.

3.7.2. Ratios of cross sections

The cross sections are proportional to decay widths and proportional to branching ratios. From the ratios of cross sections we can derive the ratios of branching ratios. The decay withs are also proportional to the other quantities, therefore we can use the theoretical decay widths to compute the expected ratios.

From the manual we obtain the theoretical hadronic width of 1732 MeV. The leptonic width should be 83.8 MeV. Therefore we expect a ratio between the hadron and each leptonic channel to be 20.7.

Using the values given in Table 3.12, we obtain a value of 9.7(5), 21.3(9) and 23(2) for electrons, muons and tauons, respectively. The values for muons and tauons is in agreement with theory. The one for the electrons is too small, which comes from the wrong analysis of the t-channel.

3.7.3. Confidence level

Least-squares fitting is the maximization of the likelihood function. The minimization of the χ^2 quantity with respect to the fit parameter vector $\boldsymbol{\lambda}$ is an equivalent problem. The χ^2 is computed with a model f and parameters $\boldsymbol{\lambda}$ from observations $\{x_i\}$ using

$$\chi^2 = \sum_i \left(\frac{x_i - f(x_i, \boldsymbol{\lambda})}{\sigma_i} \right)^2 .$$

The fitting algorithm has already found the parameters $\boldsymbol{\lambda}$ (including mass and width) for us. Now we need to compute the χ^2 from this. The four decay channels have a χ^2 each of 6.95, 9.06, 118 and 4.41.

This value without the degrees of freedom is rather worthless. Therefore we look at the "reduced χ^2" which is χ^2/dof. This quantity pictorially is the average distance of the points to the curve

Type	χ^2	χ^2/dof	p
Electrons	6.95	2.32	0.0735
Muons	9.06	3.02	0.0285
Tauons	118	39.5	0.00
Hadrons	4.41	1.47	0.220

Table 3.13.: Confidence for fits.

measured in the individual standard deviations. A value of 1 to 1.5 means that on average, the points tangent the line with the error bar. This means that the errors are not too large or small, the model fits. If the value is way smaller than 1, the errors have been overestimated. If the value is larger than 1.5, the model does not fit; points lie very far away from the curve.

Here we have seven beam energies and three model parameters, this gives dof $= 7-1-3 = 3$. The reduced χ^2 are then 2.32, 3.02, 39.5 and 1.47. Most values are quite large.

The so-called p-value gives the probability that the underlying model would produce this data or a more extreme variant of this. Therefore we want a high p-value, saying that the values that we have are quite normal for this model. A common lower bound is 0.05, everything below that will reject the model.

The p-value is computed from the χ^2 cumulative density function which is implemented as `scipy.stats.chi2.cdf`. Inserting our values for χ^2 and dof, we obtain the p-values 0.0735, 0.0285, 0.00 and 0.220.

All values are collected in Table 3.13. From the p-value we must conclude that the Breit-Wigner prescription alone is not a good description of the decays into muons and tauons when using the 0.05 threshold. For the tauons, Figure 3.9c clearly shows that a couple lie way off the curve. This does give a large χ^2 and therefore small p-value. It is not that bad for the muons, we have $p = 0.0285$ which is not *that* far away from 0.05. Looking at Figure 3.9b, one can see that the deviations are larger than in the electron and hadron channel.

3.7.4. Partial decay widths

Using the relation

$$\sigma_f^{\text{peak}} = \frac{12\pi}{M_{Z^0}^2}\frac{\Gamma_e\Gamma_f}{\Gamma_Z^2}$$

given in the manual as (2.14), we can compute the partial decay widths for the individual flavors by solving for Γ_e first and then for Γ_f. We compute the decay width of the electron via

$$\Gamma_e = M_{Z^0}\Gamma_Z\sqrt{\frac{\sigma_\mu^{\text{peak}}}{12\pi}} = 94(4)\,\text{MeV}.$$

Although the expression should use the peak cross section for the electron, we substitute the one for the muon. The rationale is simple: We know that the partial cross section of the electron is overestimated by our mistake in the cutting. Assuming the lepton universality actually holds,

	Γ_f /MeV	
Channel	Measurement	Theory
Electrons	207(12)	84.1
Muons	94(4)	84.1
Tauons	88(6)	84.1
Hadrons	2006(112)	1689

Table 3.14.: Comparison of extracted and theoretical partial widths.

we can just substitute the width into muons for the width into electrons. If we would not do this, we would end up with around 14 neutrino families. Therefore we work around the erroneous Γ_e by substituting Γ_μ for it in that one equation. We also use our own values of M_{Z^0} and Γ_Z that we obtain by averaging the fit results. This will make our result less accurate but more honest.

With the decay width into electrons, we can compute the decay widths into other flavors using the similar expression

$$\Gamma_f = \frac{M_{Z^0}^2 \Gamma_Z^2}{\Gamma_e} \frac{\sigma_f^{\text{peak}}}{12\pi} .$$

The resulting four decay widths are 207(12) MeV, 94(4) MeV, 88(6) MeV and 2006(112) MeV for electrons, muons, tauons and hadrons, respectively. The decay width into muons has not changed as we have basically used that to compute the other widths.

Our results are summed up in Table 3.14 which compares the values to the theoretical ones listed in Table 2.1 and Section 2.2. We see that the decay widths into muons and tauons are quite near, only Γ_τ has the theoretical value within one standard deviation. For the muons, we already need more than two standard deviations. As expected by now, Γ_e is quite far off. A little surprising is that Γ_{hadrons} is more than three standard deviations away from the expected value.

3.7.5. Lepton universality

Our partial cross sections at the peak are listed in Table 3.12. Lepton universality states that at high enough energy, which we have with $\sqrt{s} \simeq M_{Z^0}$, all charged leptons will be virtually massless and the weak isospin doublets behave exactly the same. This should manifest itself in exactly equal partial cross sections for the three lepton flavors.

For the muons and tauons, the cross sections are well compatible with each other. For the electrons, it is a bit more than a factor two too large, the error cannot account for that. This originates in the wrong t-channel cutting.

3.7.6. Neutrino generations

Subtracting the observed decay channels from the observed width of the Z-boson, we are missing a width of 461(52) MeV. The width of the neutrinos is $\Gamma_\nu = 167.6$ MeV (taken from Table 2.1

from the manual). The quotient gives us the number of light neutrino families, 2.7(3). This number is just a bit more than a standard deviation away from the expected value of 3. The error is quite large, but that is expected from the various uncertainties going into this quantity.

4. Conclusion

4.1. Results and discussion

We are able to determine the weak mixing angle to $\sin(\theta_w)^2 = 0.239^{+0.001}_{-0.013}$. The literature value is 0.231 and lies very well within our uncertainty.

Our analysis leads to 2.7(3) neutrino families. The current value is 3, this also lies nicely within the uncertainty.

The mass of the Z^0 is determined to be 91.15(3) GeV. Here the literature value is 91.182 GeV (taken from manual). Our value is well within the range. The corresponding width is 2.9(1) GeV. We have computed the total width to be 2443 MeV in the exercises. Our value is too high to be within the uncertainty. This is probably due to our overestimation of the scattering into electrons.

Since we have overestimated the partial cross section of the electrons, we are not able to fully show the lepton universality. However, we have assumed the lepton universality at some point and used the muonic cross section instead. The results obtained with this exchange gives us sensible results, implying that lepton universality actually holds.

4.2. Implicit assumptions

During our analysis, we have used a couple implicit assumptions.

- Errors of count experiments are $\sqrt{N}$.
- We also have assumed that the distribution of errors are Gaussian when we have used resampling. This is an assumption that would have been done anyway when using Gaussian error propagation. At least we did not have to assume that the errors are small at any point.
- The energy of the beam should have been roughly constant within one of the seven settings. From the PAW histograms we could see that is sufficiently the case.
- The Breit-Wigner prescription is only good for a narrow resonance. Otherwise one would have a violation of unitarity. As we have seen in our results, this assumption can be justified.
- We assume that the OPAL detector does not have a bias. The Monte Carlo datasets allow us to derive the bias of our cuts. If the detector is less sensible to certain decays, we would have a bias in the end as well.

As far as we know, the event rate is so high that not every single event can be recorded. Therefore there are FPGA stages which reduce the number of events dramatically. Those are constructed not to introduce a bias, but one has to ensure this.

A. PAW Histograms

A.1. Monte Carlo data

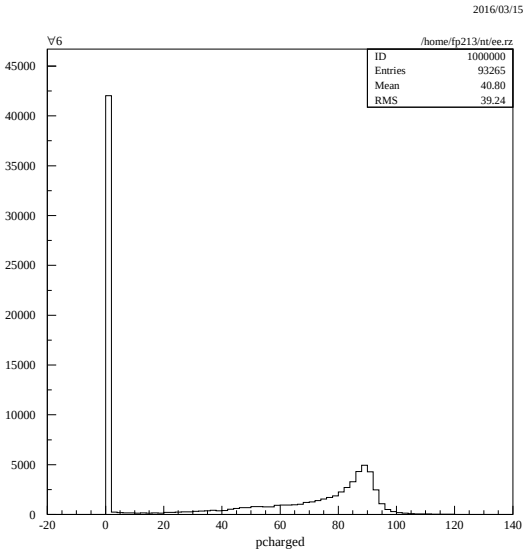

(a) Electrons

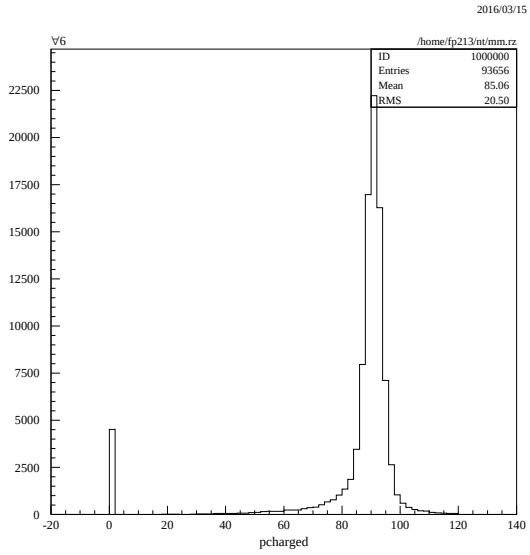

(b) Muons

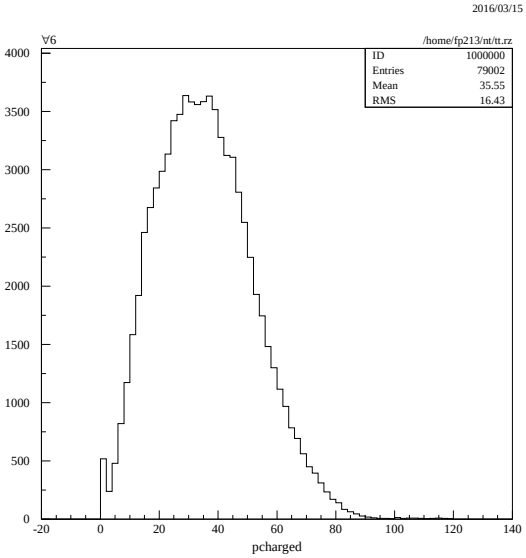

(c) Tauons

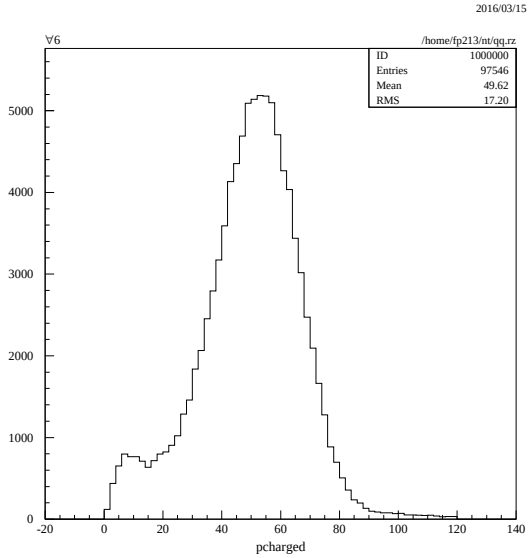

(d) Hadrons

Figure A.1.: Energy in charged tracks, p-charged, for the four decay types. Histograms generated with PAW from Monte Carlo datasets.

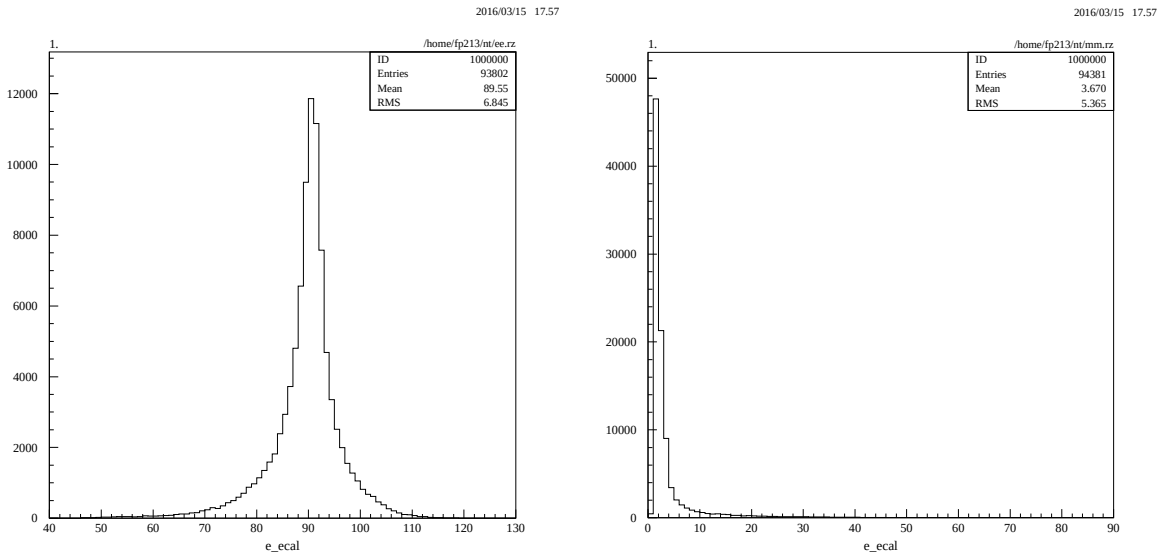

(a) Electrons (b) Muons

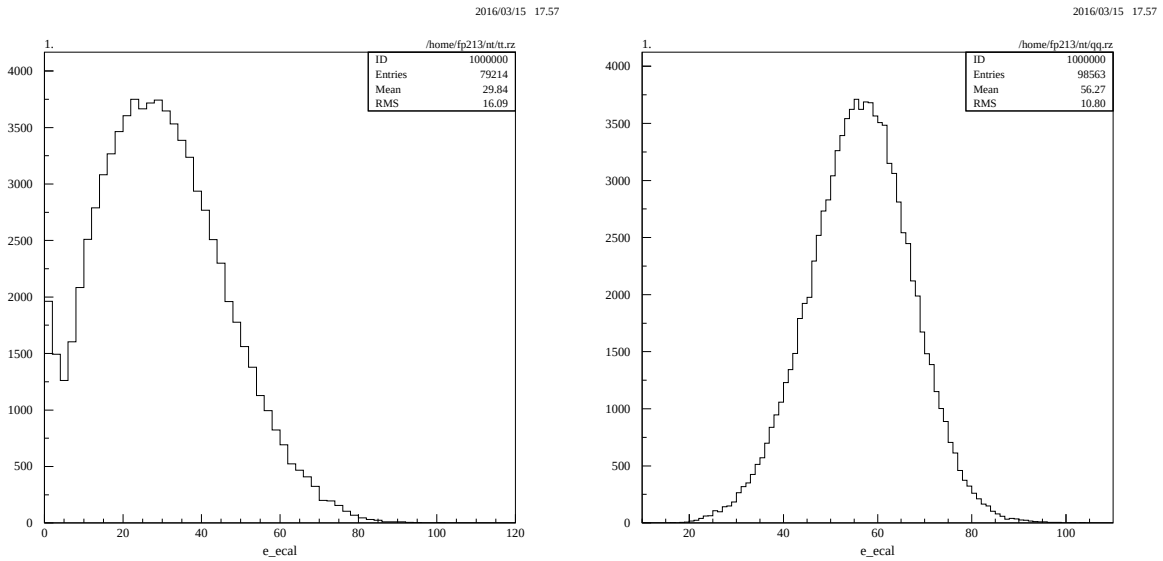

(c) Tauons (d) Hadrons

Figure A.2.: Energy deposited into the E-e-cal for the four decay types. Histograms generated with PAW from Monte Carlo datasets.

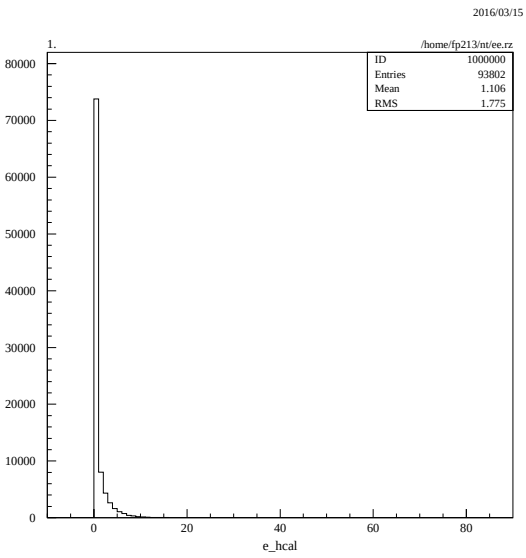

(a) Electrons

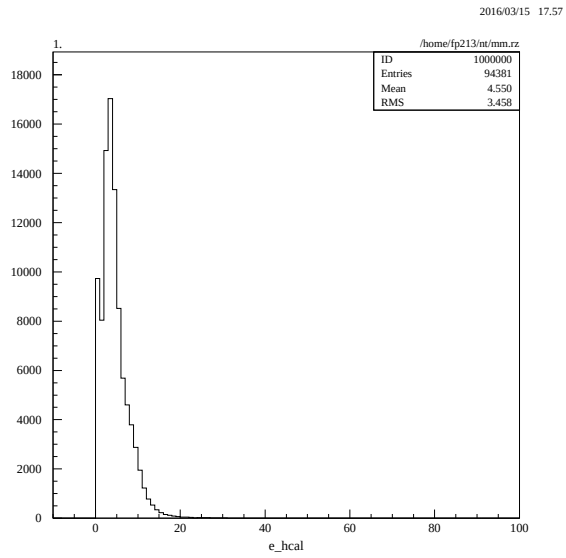

(b) Muons

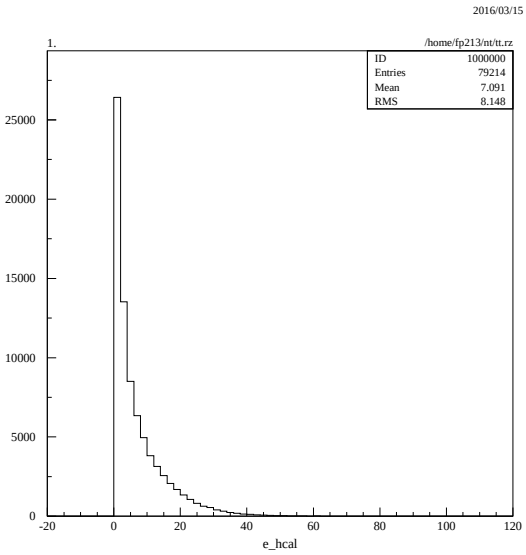

(c) Tauons

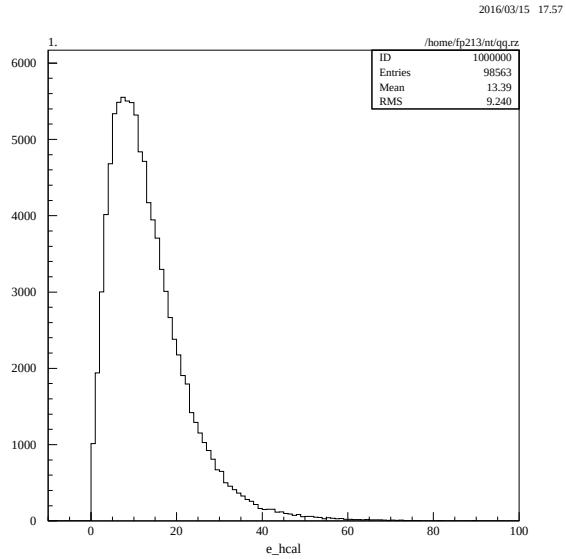

(d) Hadrons

Figure A.3.: Energy deposited into the E-h-cal for the four decay types. Histograms generated with PAW from Monte Carlo datasets.

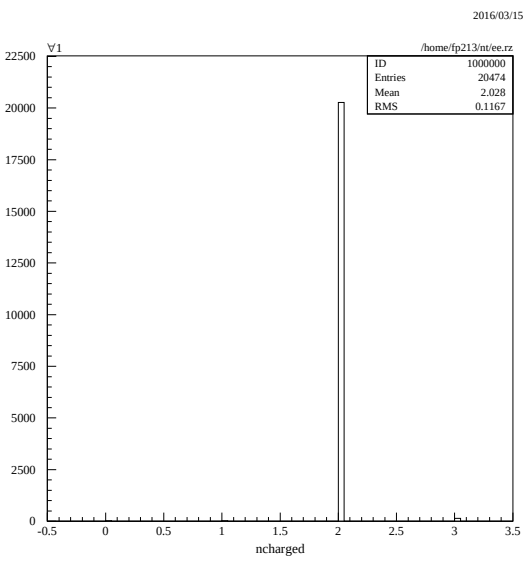

(a) Electrons with electron cut

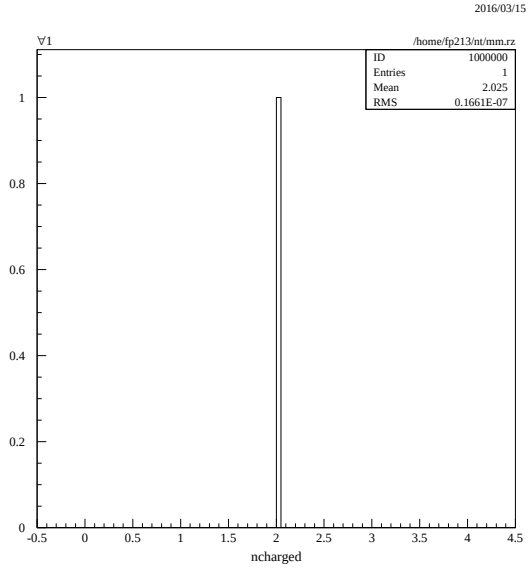

(b) Muons with electron cut

Figure A.4.: Histograms to obtain number of matched events in out cuts. Created with PAW from Monte Carlo datasets.

B. Decay width derivation

First we compute the invariant matrix element $\mathscr{M}$. Reading off the Feynman diagram, we have

$$\mathrm{i}\mathscr{M} = \epsilon^{\mu}\bar{u}^{s}(\underline{\boldsymbol{p}})\frac{\mathrm{i}g}{\cos(\theta_{\mathrm{w}})}\gamma_{\mu}\left(g_{\mathrm{v}}^{f} - g_{\mathrm{a}}^{f}\gamma_{5}\right)v^{s'}(\underline{\boldsymbol{k}}),$$

where we have used the rules given by Romão [Rom12, (D.56)]. We chose the center of mass system, as we always can for a single massive particle, and have $\underline{\boldsymbol{q}} = (\sqrt{s}, \mathbf{0})$. As the gauge boson does not have any three momentum direction, we can choose the polarization vector $\underline{\boldsymbol{\epsilon}}$ like we want. We chose it in the positive x^3-direction and have $\underline{\boldsymbol{\epsilon}} = (0,0,0,1)$. With that we can simplify the Lorentz structure a little bit and obtain

$$= \bar{u}^{s}(\underline{\boldsymbol{p}})\frac{\mathrm{i}g}{\cos(\theta_{\mathrm{w}})}\gamma_{3}\left(g_{\mathrm{v}}^{f} - g_{\mathrm{a}}^{f}\gamma_{5}\right)v^{s'}(\underline{\boldsymbol{k}}).$$

For the decay width, which we are interested in, we need the modulus squared of the matrix element. For that we need the following:

$$\begin{aligned}
&\left[\bar{u}^{s}(\underline{\boldsymbol{p}})\gamma_{3}\left(g_{\mathrm{v}}^{f} - g_{\mathrm{a}}^{f}\gamma_{5}\right)v^{s'}(\underline{\boldsymbol{k}})\right]^{\dagger} \\
&\quad = v^{s'}(\underline{\boldsymbol{k}})^{\dagger}\left(g_{\mathrm{v}}^{f} - g_{\mathrm{a}}^{f}\gamma_{5}^{\dagger}\right)\gamma_{3}^{\dagger}\gamma_{0}u^{s}(\underline{\boldsymbol{p}}) \\
&\quad = \underbrace{v^{s'}(\underline{\boldsymbol{k}})^{\dagger}\gamma_{0}}\,\underbrace{\gamma_{0}\left(g_{\mathrm{v}}^{f} - g_{\mathrm{a}}^{f}\gamma_{5}^{\dagger}\right)\gamma_{0}}\,\underbrace{\gamma_{0}\gamma_{3}^{\dagger}\gamma_{0}}\,u^{s}(\underline{\boldsymbol{p}}) \\
&\quad = \bar{v}^{s'}(\underline{\boldsymbol{k}})\left(g_{\mathrm{v}}^{f} + g_{\mathrm{a}}^{f}\gamma_{5}\right)\gamma_{3}u^{s}(\underline{\boldsymbol{p}}) \\
&\quad = \bar{v}^{s'}(\underline{\boldsymbol{k}})\gamma_{3}\left(g_{\mathrm{v}}^{f} - g_{\mathrm{a}}^{f}\gamma_{5}\right)u^{s}(\underline{\boldsymbol{p}}).
\end{aligned}$$

Now we can write the modulus squared of the matrix element

$$|\mathscr{M}|^{2} = \frac{g^{2}}{\cos(\theta_{\mathrm{w}})^{2}}\bar{v}^{s'}(\underline{\boldsymbol{k}})\gamma_{3}\left(g_{\mathrm{v}}^{f} - g_{\mathrm{a}}^{f}\gamma_{5}\right)u^{s}(\underline{\boldsymbol{p}})\bar{u}^{s}(\underline{\boldsymbol{p}})\gamma_{3}\left(g_{\mathrm{v}}^{f} - g_{\mathrm{a}}^{f}\gamma_{5}\right)v^{s'}(\underline{\boldsymbol{k}}).$$

As the detector is not sensitive to the spin of the resulting fermions, we need to sum over all the final state spin configurations s and s'. This will give us a fermion trace,

$$\sum_{\text{spins}}|\mathscr{M}|^{2} = \frac{g^{2}}{\cos(\theta_{\mathrm{w}})^{2}}\operatorname*{tr}_{\text{Dirac}}\left(\underline{\boldsymbol{k}}\gamma_{3}\left(g_{\mathrm{v}}^{f} - g_{\mathrm{a}}^{f}\gamma_{5}\right)\underline{\boldsymbol{p}}\gamma_{3}\left(g_{\mathrm{v}}^{f} - g_{\mathrm{a}}^{f}\gamma_{5}\right)\right),$$

where we have neglected the masses of the fermions. The second parentheses with γ_5 can be anticommuted twice and be collapsed with the first one. We have

$$= \frac{g^2}{\cos(\theta_\mathrm{w})^2} \operatorname*{tr}_{\text{Dirac}} \left(\underline{\boldsymbol{k}} \gamma_3 \left(g_\mathrm{v}^f - g_\mathrm{a}^f \gamma_5 \right)^2 \underline{\boldsymbol{p}} \gamma_3 \right),$$

where we can now simplify this. As an aside, we have

$$\left(g_\mathrm{v}^f - g_\mathrm{a}^f \gamma_5 \right)^2 = (g_\mathrm{v}^f)^2 + (g_\mathrm{a}^f)^2 - 2 g_\mathrm{v}^f g_\mathrm{a}^f \gamma_5 .$$

The square of γ_5 is just the unit matrix in Dirac space. The term with γ_5 will drop out as the trace identity contains the Levi-Civita symbol $\epsilon_{\mu\nu\rho\gamma}$ which will be zero if two of the indices are 3, as we have in our case. Therefore we can directly drop that term. As the parentheses does not contain any further Dirac structure, we can pull it out front and obtain

$$= \frac{g^2}{\cos(\theta_\mathrm{w})^2} \left((g_\mathrm{v}^f)^2 + (g_\mathrm{a}^f)^2 \right) \operatorname*{tr}_{\text{Dirac}} \left(\underline{\boldsymbol{k}} \gamma_3 \underline{\boldsymbol{p}} \gamma_3 \right).$$

Using a trace identity like the one given by Peskin and Schroeder [PS95, (A.27)], we obtain

$$= \frac{4g^2}{\cos(\theta_\mathrm{w})^2} \left((g_\mathrm{v}^f)^2 + (g_\mathrm{a}^f)^2 \right) (2k_3 p_3 + \underline{\boldsymbol{k}} \cdot \underline{\boldsymbol{p}}).$$

This is our final form of the matrix element.

The decay width is given by additional factors and an integration over phase space. We have

$$\Gamma_f = \frac{1}{2M_{\mathrm{Z}^0}} (2\pi)^4 \int \frac{\mathrm{d}^3 p}{(2\pi)^3 2E_{\underline{\boldsymbol{p}}}} \frac{\mathrm{d}^3 k}{(2\pi)^3 2E_{\underline{\boldsymbol{k}}}} \delta^4(\underline{\boldsymbol{q}} - \underline{\boldsymbol{k}} - \underline{\boldsymbol{p}}) |\mathscr{M}|^2 .$$

We simplify the factors and insert the matrix element and get

$$= \frac{1}{32\pi^2 M_{\mathrm{Z}^0}} \int \frac{\mathrm{d}^3 p}{E_{\underline{\boldsymbol{p}}}} \frac{\mathrm{d}^3 k}{E_{\underline{\boldsymbol{k}}}} \delta^4(\underline{\boldsymbol{q}} - \underline{\boldsymbol{k}} - \underline{\boldsymbol{p}}) \frac{4g^2}{\cos(\theta_\mathrm{w})^2} \left((g_\mathrm{v}^f)^2 + (g_\mathrm{a}^f)^2 \right) (2k_3 p_3 + \underline{\boldsymbol{k}} \cdot \underline{\boldsymbol{p}}).$$

Then we simplify even more and obtain

$$= \frac{1}{8\pi^2 M_{\mathrm{Z}^0}} \frac{g^2}{\cos(\theta_\mathrm{w})^2} \left((g_\mathrm{v}^f)^2 + (g_\mathrm{a}^f)^2 \right) \int \frac{\mathrm{d}^3 p}{E_{\underline{\boldsymbol{p}}}} \frac{\mathrm{d}^3 k}{E_{\underline{\boldsymbol{k}}}} \delta^4(\underline{\boldsymbol{q}} - \underline{\boldsymbol{k}} - \underline{\boldsymbol{p}}) (2k_3 p_3 + \underline{\boldsymbol{k}} \cdot \underline{\boldsymbol{p}}).$$

The total energy-momentum conserving Dirac-distribution can be split into time-like and space-like part. In the center-of-mass frame, this gives us

$$\begin{aligned} &= \frac{1}{8\pi^2 M_{\mathrm{Z}^0}} \frac{g^2}{\cos(\theta_\mathrm{w})^2} \left((g_\mathrm{v}^f)^2 + (g_\mathrm{a}^f)^2 \right) \\ &\quad \times \int \frac{\mathrm{d}^3 p}{E_{\underline{\boldsymbol{p}}}} \frac{\mathrm{d}^3 k}{E_{\underline{\boldsymbol{k}}}} \delta(\sqrt{s} - E_{\underline{\boldsymbol{k}}} - E_{\underline{\boldsymbol{p}}}) \delta^3(\boldsymbol{k} + \boldsymbol{p}) (2k_3 p_3 + \underline{\boldsymbol{k}} \cdot \underline{\boldsymbol{p}}), \end{aligned}$$

which suggests the following change in variables:

$$\boldsymbol{a} := \boldsymbol{p} + \boldsymbol{k}\,, \qquad \boldsymbol{b} := \frac{\boldsymbol{p} - \boldsymbol{k}}{2}\,.$$

The Jacobian of this transformation is unity. The $\delta^3(\boldsymbol{k}+\boldsymbol{p})$ will become $\delta^3(\boldsymbol{a})$. This will set $\boldsymbol{a}$ to $\boldsymbol{0}$ in the $\int \mathrm{d}^3 a$ integral. So far we have

$$= \frac{1}{8\pi^2 M_{\mathrm{Z}^0}} \frac{g^2}{\cos(\theta_{\mathrm{w}})^2} \left((g_{\mathrm{v}}^f)^2 + (g_{\mathrm{a}}^f)^2\right) \int \frac{\mathrm{d}^3 b}{E_{\boldsymbol{p}} E_{\boldsymbol{k}}} \delta(\sqrt{s} - E_{\boldsymbol{k}} - E_{\boldsymbol{p}})(2k_3 p_3 + \underline{\boldsymbol{k}} \cdot \underline{\boldsymbol{p}})\,.$$

Now we have to replace k and p with b. We have $\boldsymbol{p} = \boldsymbol{b}$ and $\boldsymbol{k} = -\boldsymbol{b}$. Their magnitude is the same, which is expected in the center-of-mass frame in a two body decay. This simplifies the relations to

$$= \frac{1}{8\pi^2 M_{\mathrm{Z}^0}} \frac{g^2}{\cos(\theta_{\mathrm{w}})^2} \left((g_{\mathrm{v}}^f)^2 + (g_{\mathrm{a}}^f)^2\right) \int \frac{\mathrm{d}^3 b}{E_{\boldsymbol{b}}^2} \delta(\sqrt{s} - 2E_{\boldsymbol{b}})(-2b_3 b_3 + E_{\boldsymbol{b}}^2 + \boldsymbol{b} \cdot \boldsymbol{b})\,.$$

As we have massless particles, we have $E_{\boldsymbol{b}} = |\boldsymbol{b}|$. We change into spherical coordinates in $\boldsymbol{b}$ and obtain

$$\begin{aligned} &= \frac{1}{4\pi M_{\mathrm{Z}^0}} \frac{g^2}{\cos(\theta_{\mathrm{w}})^2} \left((g_{\mathrm{v}}^f)^2 + (g_{\mathrm{a}}^f)^2\right) \\ &\quad \times \int \mathrm{d}b\, b^2 \int \mathrm{d}\cos(\theta)\, \frac{1}{b^2} \delta(\sqrt{s} - 2b)(-2b^2 \cos(\theta)^2 + b^2 + b^2)\,, \end{aligned}$$

where we have performed $\int \mathrm{d}\phi = 2\pi$ already as we do not have any explicit ϕ-dependence. The radial integration will set $b = \sqrt{s}/2$. In our case $s = M_{\mathrm{Z}^0}^2$ and we have

$$= \frac{M_{\mathrm{Z}^0}}{16\pi} \frac{g^2}{\cos(\theta_{\mathrm{w}})^2} \left((g_{\mathrm{v}}^f)^2 + (g_{\mathrm{a}}^f)^2\right) \int \mathrm{d}\cos(\theta)\,(-2\cos(\theta)^2 + 2)\,.$$

The angular integration gives $(-4/3 + 4) = 8/3$, so we get

$$= \frac{M_{\mathrm{Z}^0}}{6\pi} \frac{g^2}{\cos(\theta_{\mathrm{w}})^2} \left((g_{\mathrm{v}}^f)^2 + (g_{\mathrm{a}}^f)^2\right)\,.$$

Replacing g^2 with $8M_{\mathrm{W}}^2 G_{\mathrm{F}}/\sqrt{2}$ (see Equation (2.1) from the manual) and using $M_{\mathrm{W}} = M_{\mathrm{Z}^0}\cos(\theta_{\mathrm{w}})$ (see (2.3)), we will obtain

$$= \frac{2\sqrt{2}}{3\pi} G_{\mathrm{F}} M_{\mathrm{Z}^0}^3 \left((g_{\mathrm{v}}^f)^2 + (g_{\mathrm{a}}^f)^2\right)\,.$$

For quarks, we also need to sum over all the colors, which just gives the factor N_{c}^f for the given flavor f.

$$= 8\frac{N_{\mathrm{c}}^f \sqrt{2}}{12\pi} G_{\mathrm{F}} M_{\mathrm{Z}^0}^3 \left((g_{\mathrm{v}}^f)^2 + (g_{\mathrm{a}}^f)^2\right)\,.$$

Except for a missing factor $1/8$ up front, this is the same as Equation (2.12) given in the manual. In the derivation, we have an angular dependency of $1 - \cos(\theta)$ which also looks strange. Both errors are probably related.

Bibliography

[PS95] Michael E. Peskin and Daniel V. Schroeder. *An Introduction to Quantum Field Theory*. Westview Press, 1995. ISBN: 978-0-201-50397-5.

[Rom12] Jorge C. Romão. *Feynman Rules for the Standard Model*. Dec. 2012. URL: http://porthos.ist.utl.pt/CTQFT/files/SM-FeynmanRules.pdf.